Title: Population coding of auditory space in the dorsal inferior colliculus persists with altered binaural cues

Running title: Spatial population codes of shell IC neurons

Meike M. Rogalla[1*†], Gunnar L. Quass[1†], Harry Yardley[1], Clara Martinez-Voigt[1], Alexander N. Ford[1], Gunseli Wallace[1], Deepak Dileepkumar[1], Gabriel Corfas[1], Pierre F. Apostolides[1,2*]

[1] Kresge Hearing Research Institute & Department of Otolaryngology – Head & Neck Surgery

[2] Department of Molecular and Integrative Physiology

University of Michigan Medical School, Ann Arbor, United States

* Correspondence: meike.marie.rogalla@uni-oldenburg.de or pierre.apostolides@umich.edu

[†]Present Affiliations

MMR: Department of Neuroscience, Division of Animal Physiology and Behavior, School of Medicine and Health Sciences, Cluster of Excellence Hearing4all, Carl von Ossietzky University Oldenburg

GLQ: x

Author contributions: MMR and PFA designed the research. MMR, CMV, and ANF conducted surgeries. MMR and HY collected imaging data. MMR and DD designed the sound delivery system. MMR and GW collected ABR data under the supervision of GC. MMR, GLQ, and PFA analyzed the data and interpreted results. MMR, GLQ, and PFA wrote the paper.

Acknowledgements: The authors thank Stephen F. Wollgast and Dr. Rainer Beutelmann for the support with sound delivery hard- and software, and for their helpful input regarding the experimental design; Dr. Michael T. Roberts for sharing sound delivery code and critical comments on the manuscript; Jordyn E. Czarny and Hannah M. Oberle for the support with mouse handling and animal care. This work was supported by a Deutsche Forschungsgemeinschaft (DFG) Walter Benjamin Fellowship awarded to MMR (RO 6660/1-1:1) and a National Institutes of Health grant to PFA (NIH/NIDCD R01DC019090).

Abstract (246 words)

Sound localization is critical for real-world hearing, such as segregating overlapping sound streams. For optimal flexibility, central representations of auditory space must adapt to peripheral changes in binaural cue availability, such as following asymmetric hearing loss in adulthood. However, whether the mature auditory system can reliably encode spatial auditory representations upon abrupt changes in binaural input is unclear. Here we use 2-photon Ca^{2+} imaging in awake head-fixed mice to determine how the higher-order "shell" layers of the inferior colliculus (IC) encode sound source location in the frontal azimuth, under binaural conditions and after acute monaural hearing loss induced by an ear plug ipsilateral to the imaged hemisphere. Spatial receptive fields were typically broad and not exclusively contralateral: Neurons responded reliably to multiple positions in the contra- and ipsi-lateral hemifields, with preferred positions tiling the entire frontal azimuth. Ear plugging broadened receptive fields and reduced spatial selectivity in a subset of neurons, in agreement with an inhibitory influence of ipsilateral sounds. However ear plugging also enhanced spatial tuning and/or unmasked receptive fields in other neurons, shifting the distribution of preferred angles ipsilaterally with minimal impact on the neuronal population's overall spatial resolution; these effects occurred within 2 hours of ear plugging. Consequently, linear classifiers trained on fluorescence data from control and ear-plugged conditions had similar classification accuracy when tested on held out data from within, but not across hearing conditions. Spatially informative neuronal population codes therefore arise rapidly following monaural hearing loss, in absence of overt experience.

Introduction

Navigating the environment relies upon internal representations of external space, which are thought to arise via the coordinated activity of neuron populations (Fitzpatrick et al., 1997; Gleiss et al., 2019; Robinson et al., 2020; Kira et al., 2023). Hearing is a particularly important sense for spatial processing: The location and movement trajectory of distant or visually obscured objects can be inferred in ego- and allo-centric reference frames from sound alone (Bergan et al., 2005; Hoy et al., 2016; Town et al., 2017;

Amaro et al., 2021), conferring a survival advantage for predator and prey alike. However, to be optimally flexible, any population code of auditory space must be capable of compensating for peripheral changes that might occur across lifetime, such as degradation of auditory information caused by hearing loss. Yet, little is known about the flexibility of neuronal populations to encode spatial auditory representations. Additionally, we do not know the extent to which such population codes can accommodate abrupt changes in afferent input.

In contrast to other sensory modalities like vision or touch, the auditory periphery lacks an explicit representation of space at the receptor level. Thus, sound source location must be derived centrally from brainstem circuits that integrate binaural cues - timing and level differences of sound waves at the two ears- as well as monaural cues, such as the direction-dependent filtering of sound waves via pinnae and head shape (For reviews see Grothe et al., 2010; Yin et al., 2019). These early computations provide the substrate for spatial selectivity in midbrain and forebrain circuits, which is thought to arise via binaural interactions: Sound information from the ear in the preferred hemifield generates net synaptic excitation in midbrain/forebrain circuits, whereas sound from the non-preferred ear is net inhibitory and constrains spatial selectivity to the preferred hemifield (Kuwada et al., 1997; Sanes et al., 1998; Breebaart et al., 2001; Ono and Oliver, 2014). This spatial selectivity towards one hemifield typically arises as contralateral dominance: Single neurons preferentially respond to sounds in the contralateral ear and are inhibited by sound from the ipsilateral side (Middlebrooks, 1987; Park and Pollak, 1993a; Klug et al., 1995, 1999; Day and Delgutte, 2013; Grothe and Pecka, 2014). Consequently, monaural hearing loss in the non-preferred ear generally broadens the receptive fields of spatially tuned midbrain and forebrain single neurons and degrades their spatial selectivity (Knudsen and Konishi, 1980; Palmer and King, 1985; Middlebrooks, 1987; Samson et al., 1994; Gooler et al., 1996a; Grant and Binns, 2003a); qualitatively similar results are seen with pharmacological block of synaptic inhibition (Moore and Caspary, 1983; Park and Pollak, 1993b, 1994; Klug et al., 1995; Sanes et al., 1998; Klug et al., 1999; Burger and Pollak, 2001; Lu and Jen, 2003). These results suggest a physiological basis for classic observations that acute, monaural hearing loss drastically impairs sound localization in animals and humans (Knudsen et al., 1984a; Hine

et al., 1994; Hofman et al., 1998; Bergan et al., 2005; Baguley et al., 2006; Bajo et al., 2010; Snapp and Ausili, 2020): Population level representations of auditory space are profoundly degraded following acute monaural hearing loss, owing to a large-scale broadening of spatial selectivity seen in single neuron recordings.

Interestingly, humans and animals can re-learn to localize sounds following chronic monaural hearing loss if provided with appropriate behavioral training (Bauer et al., 1966; Florentine, 1976a; Musicant and Butler, 1980; Knudsen et al., 1984b; Kacelnik et al., 2006; Bajo et al., 2010; Firszt et al., 2015; Keating et al., 2016; Bajo et al., 2019). This re-learning may occur via a functional remapping of associations between altered binaural cues and apparent spatial location (Knudsen et al., 1984a; Wright and Fitzgerald, 2001), or via a re-weighting of unperturbed, monaural spectral cues derived from the intact ear (Hofman et al., 1998; Keating et al., 2016). Given that monaural occlusion broadens spatial receptive fields of single neurons, any re-learning presumably depends on central plasticity mechanisms to refine a degraded spatial code and stamp in new population-level representations of sound source location. However, this hypothesis has not been directly tested, as it requires tracking the spatial selectivity of large groups of neurons before and after monaural hearing loss; this feat is difficult via traditional physiological approaches.

We address this knowledge gap by studying population-level coding of sound source location in the higher-order non-lemniscal “shell” layers of the inferior colliculus (IC), an auditory midbrain region important for sound localization behavior (Masterton et al., 1968; Jenkins and Masterton, 1982; Zrull and Coleman, 1997; Litovsky et al., 2002; Champoux et al., 2007; Kwee et al., 2017). We focus specifically on the shell IC subregion because classic studies suggest it as an early locus of experience-dependent plasticity for spatial auditory representations (Brainard and Knudsen, 1993; Mogdans and Knudsen, 1993; Gold and Knudsen, 2000; Knudsen, 2004; Bajo et al., 2010, 2019), and because it provides a major auditory input to brain circuits involved in learned and innate behaviors (Ledoux et al., 1987; King et al., 1998; Winer et al., 1998; Xiong et al., 2015; Chen et al., 2018; Cai et al., 2019; Goyer et al., 2019; Barsy

et al., 2020; Ito et al., 2020; Valtcheva et al., 2023). Using 2-photon Ca^{2+} imaging in awake, head-fixed mice, we measured the spatial receptive fields of shell IC neurons under binaural conditions and immediately after abrupt monaural occlusion ipsilateral to the recorded hemisphere. Spatial tuning was surprisingly diverse under binaural conditions, with peak responses in either the contralateral or ipsilateral hemifields. Consequently, a population-level representation of auditory space tiled the entire frontal azimuth and enabled reliable decoding of all tested sound source locations using linear classifiers. Monaural occlusion broadened spatial receptive fields in a subset of neurons ipsilateral to the occlusion, in agreement with a net inhibitory role for ipsilateral acoustic signals. Contrary to our expectations however, a significant fraction of neurons maintained their spatial tuning or remapped their receptive fields to new preferred locations. A reliable population code for horizontal space thus emerges in the shell IC upon a dramatic change in cue availability, albeit one reliant on distinct subsets of neurons from those under binaural conditions. Abrupt peripheral changes therefore rapidly switch midbrain spatial population codes in apparent absence of extensive experience. Thus, adaptive plasticity mechanisms compensating for altered binaural inputs (Moore and Irvine, 1981; Gold and Knudsen, 1999, 2000; Keating et al., 2013; Thornton et al., 2021) may operate on faster timescales than previously appreciated.

Methods

Animal subjects and handling

All procedures were approved by the University of Michigan's Institutional Animal Care and Use Committee and carried out in accordance with the NIH's guide for the care and use of laboratory animals. We used a total of 10 normal hearing mice (5 female 5 male, 10-14 weeks at the time of surgery), F1 offspring of C57.Bl6/J x CBA/CaJ breeders (CBA(♂): 000654; C57(♀): 000664, the Jackson Laboratories), bred in our colony. N = 9 mice were employed for imaging experiments and one mouse was used solely for ABR testing ear plug efficacy. Mice were single-housed with visual and olfactory contact to neighboring animals at a reversed 12/12-hour dark-light cycle, food and water were provided ad libitum. Cages were equipped with standardized enrichment (running wheels, shelter, and two different forms of nest-building material) to reduce stereotypic behavior and stress. Experiments were only conducted during the dark period, usually once/day which was extended to 2 sessions in the case of plugging days. Handling by the experimenter began at least 10 days following surgery and comprised 4-10 sessions of habituation to the Plexiglas seating tube in which mice sit during head fixation (see also Guo et al., 2014). During these sessions, mice were allowed to explore the tube in the cage, followed by sessions of exploring the tube in the hand of the experimenter. In the last 2 sessions, mice were carefully fixated by holding the head bar for a few seconds.

Surgeries

Surgeries were conducted between 10-14 weeks of age. Mice were deeply anesthetized using 5% isoflurane in an induction chamber and then transferred to a stereotaxic frame (M1430, Kopf Instruments). Mice received 5 mg/kg carprofen as a preoperative analgesic subcutaneously (Rimadyl, Zoetis). Surgery was performed on a closed-loop heating pad (M55 Harvard Apparatus) to maintain body temperature at 37°C degrees. The head was fixed using non-rupture ear bars (922, Kopf), the eyes were covered with lubricant, and anesthesia was maintained at 1.5-2 % (flow rate: 0.8-1 L/min). A small incision was made near the coronal suture and extended caudally until full exposure of the interparietal bone. Following application of lidocaine (2 %, Akorn) to wound margins, the periost was removed and the skull

was adjusted by leveling the position of Lambda and Bregma (z). A circular craniotomy (2.25-2.5 Ø) was carefully drilled above the left IC (x = -1000 µm; y = -900 µm, relative to Lambda) and the viral construct for the expression of the Ca^{2+} indicator GCaMP6f (n = 2, pAAV1.Syn.GCaMP6f.WPRE.SV40, Addgene, titer order of magnitude 10^{12}) or GCaMP8s (n = 7, pAAV1.Syn.GCaMP8s.WPRE, Addgene, titer order of magnitude 10^{12}) was pressure ejected at 4 sites ~200 µm below the dura (25 nl each; 100 nl total) across the medial lateral axis of the IC using an automated injection system (Nanoject III, Drummond). A custom-made cranial window consisting of three circular 2 mm glass coverslips stacked fixed to a 4 mm diameter glass coverslip (Potomac) via optical adhesive (#71, Norland) was then inserted in the craniotomy such that the 3x stack faced inside and made contact with the dura above the dorsal shell IC. The outer rim of the window was affixed to the skull using cyanoacrylate glue (Loctite). The entire skull was covered first with cyanoacrylate glue, followed by orthodontic acrylic resin (Ortho-Jet, Lang). A custom-made titanium head bar was placed perpendicular to the window surface and encased in resin. The bar was placed far behind pinnae to leave pinnae fully exposed to allow for naturalistic binaural and monaural spectral cues. During resin application, ear bars were already loosened, and isoflurane was lowered to ~1-1.5 % to shorten immediate post-surgery recovery and to reduce the risk of potential respiratory inhibition, a side effect of buprenorphine (0.03 mg/kg, PAR pharmaceutical), which was administered subcutaneously at the end of the surgery to reduce pain during the immediate recovery. Mice were allowed to recover in a clean cage on a heating pad for approximately 1 hour and were provided with a purified high energy dietary supplement (DietGel Boost, Clear H2O) to support recovery. Following 24 and 48 hours, mice received additional injections of carprofen. Wellbeing and surgical sites were closely monitored for 7 days following surgery.

Sound delivery system

We developed a movable acoustic delivery system consisting of a servo motor (2000 Series Dual Mode Servo 25-2, Torque) equipped with a 30 cm arm (33-hole aluminum flat beam, Actobotics), carrying the speaker (XT25SC90-04, Peerless by Tymphany) at the distal end via a custom 3D printed mount. The servo was integrated into a servo block (25 tooth spline, hub shaft, Torque) to isolate the radial load and

centered under the head of the head-fixed animal, enabling 180° speaker rotation within the frontal horizontal field. Servo movement was controlled via pulse-width modulation signals generated in MATLAB and delivered via an analog headphone channel on a high-fidelity sound card (Fireface UFX+, RME). The commands were fed into a custom-made signal conditioning circuit to smooth and amplify the output signal to 5V. Duty cycles for each position were carefully calibrated to an accuracy of 1-2°. Trial-to-trial positional accuracy was additionally controlled using a "hardwired" closed loop control of speaker position using a microcontroller (Arduino UNO, Arduino AG) and a photo interrupter mounted on a 3D printed slotted disc, with each slot corresponding to the specific speaker angles used in a particular imaging session. Servo movements occurred selectively during the inter-trial interval, at least 15 seconds prior to data acquisition of each trial.

The speaker was placed at the distal end of the servo arm, 30 cm away from the animal's head. Acoustic stimuli (4-35 kHz frozen broad-band noise with 5 ms on/offset cosine ramps, 500 ms duration) were generated in Matlab (192 kHz sampling rate) and presented at 65 dB SPL via a high-fidelity sound card (Fireface UFX+, RME) and 200 W power amplifier (SLA-2, ART). Sound-servo positions were calibrated from -90° to 90° (zeroed on midline) in steps of 30°, resulting in 7 independent speaker positions. The speaker was calibrated at each position using a 1/4" pressure-field microphone (CCLD pressure-field, Type 4944-A, Bruel & Kjaer). The microphone was positioned using a custom 3D-printed attachment for the head bar holders which centered the microphone at the approximated center of the animal's head, with the microphone membrane perpendicular to the horizon.

2-photon Ca^{2+} imaging

Experiments were performed in darkness and lasted max. 45 min/session. Each imaging trial consisted of 3 sound presentations at a specific angle, with 5 seconds between each sound presentation. Following each imaging trial, the speaker was moved to a new position, this resulted in a recording trial length of 19 seconds and a total of 30 sound presentations/angle. Each trial was followed by a 19 s inter-trial-interval in which the servo was addressed for 4 s, with actual movement time varying due to trial-to-trial

position differences. A 15 s “silent” laser-off period followed motor movement to minimize overlap between sound responses driven by the motor and sound presentation on the next trial.

Mice were placed in a Plexiglas tube and head fixed on a custom-build rig. The whole experimental setup (microscope, head-fixation system, and sound delivery system) was placed on an optical table and surrounded by a sound attenuating double-walled booth, lined with foam. Images were recorded via a two-photon microscope (Sutter Instruments) at a frame rate of 30 Hz and a resolution of 512x512 pixels using a resonance scanner, a 16x water immersion objective (Nikon, 0.8 NA, 3 mm working distance), and a GaAsP photomultiplier tube (Hamamatsu Photonics). GCaMP was excited at 920 nm using a Titanium-Sapphire laser (Chameleon Ultra 2, Coherent) which was positioned on the air table outside of the booth.

Ear plugging

Mice underwent two separate imaging sessions (pre- and post-plug) on the day of ear-plugging. To reduce stress, we waited at least 1.5 hours between pre-plug session and actual ear plugging. Animals were anesthetized using isoflurane and placed on the bite bar and heating pad of a rotatable stereotaxic frame without the support of ear bars. Here, anesthesia was maintained between 1-1.5 % isoflurane due to the non-invasive nature of the procedure and to achieve a rapid recovery. Lubricant was applied to the animals’ eyes and bite bar and gas mask were carefully rotated while constantly adjusting the posture of the animals’ body until the left ear (ipsilateral to the IC window) was exposed and faced upwards. Mice received a shot of carprofen (2.5 mg/kg s.c.) to reduce any potential discomfort associated with plug placement and thus to reduce scratching and grooming behavior to avoid early plug loss. Both pinna and distal portion of the ear canal were cleaned with ethanol and fur that reached into the ear canal and pinna was removed. The appearance of the ear canal and the tympanic membrane were evaluated using a small digital otoscope (Teslong). A standard human earplug (Mack’s Ultra Soft Foam Earplugs – NRR 33 dB, McKoen) was cut in a cone-like shape with an outside facing diameter of ~5 mm and a maximum length of 3 mm. The plug was superficially wiped with ethanol, dried, compressed using forceps, carefully

inserted into the ear canal, and released. Following expansion, the plug was checked for a tight seal around the entire edge before a skin-friendly 2-component silicone rubber (BodyDouble Fast, Smooth-On Inc.) was applied to cover the foam plug. The mouse was rotated back and then remained on the frame to allow the hardening of the silicone rubber (~7 min). Post-plug imaging data were collected following a minimum of 1.5 hours recovery.

To ensure that any change in spatial responses were due to monaural hearing loss rather than anesthetic delivery or representational drift (Rule et al., 2019; Deitch et al., 2021; Aitken et al., 2022), N=2 control mice underwent a similar anesthetic induction and imaging regime as described above but were not fitted with an earplug.

We tested the efficacy of our ear plug approach by measuring auditory brainstem responses (ABR) in two of the mice of the experimental group and one naïve mouse without a head bar. ABRs were obtained via an EPL Cochlear Function Test Suite (Eaton-Peabody Laboratories, Massachusetts Eye and Ear, as described in Cassinotti et al., 2022). Animals were anesthetized with ketamine (initial 10 mg/ kg, maintenance 2.5 mg/kg) and xylazine (initial 0.083 mg/kg, maintenance 0.01 mg/kg). Anesthesia depth was confirmed via toe pinch and anesthetic maintenance doses were provided as needed. Subcutaneous needle recording electrodes were placed behind the ear, and a reference electrode was placed at the vertex. A ground electrode was additionally placed at the tail. Electrode signals were bandpass filtered (300 Hz to 3 kHz) and amplified 10,000-fold. Sound was monaurally delivered directly into the ear canal (unplugged ears) or near field in front of the plug. Recordings were performed using National Instruments input/output boards hardware. To determine hearing thresholds at different sound frequencies, tone pips (5 ms, 0.5 ms cosine ramps at onset and offset) were presented at 8, 16, and 32 kHz. The intensity was varied between 10 and 80 dB SPL in 5 dB steps. An automatic online artifact rejection algorithm discarded trials with muscle potential artifacts according to a preset threshold. ABR data were recorded continuously and saved for offline analyses. For every stimulus at least 400 artifact free trials were recorded. Thresholds at individual sound frequencies were determined by eye from the average stimulus-

aligned traces at each frequency as the lowest level that evoked an ABR. If no response could be evoked up to 80 dB SPL, threshold was set to 80 dB.

Imaging data analysis

We used the Python version of Suite2p (Pachitariu et al., 2017) to motion correct the raw data and extract fluorescence time series from regions of interests (ROIs) corresponding to individual IC neurons. Datasets were manually curated to exclude neurites and overlapping ROIs. Raw fluorescence traces were converted to ΔF/F by dividing the fluorescence by the mean baseline intensity for each trial (1 s prior to sound onset; 30 frames). The surrounding neuropil signal was scaled by a factor of 0.7 and subtracted and traces were smoothed using a 5-frame gaussian kernel. ΔF/F traces were then further analyzed using custom MATLAB code (version 2021a & 2022b). To determine significantly responding ROIs, we used a bootstrapping procedure based on the trial-by-trial autocorrelation of ΔF/F waveforms on similar trial types (Geis et al., 2011; Wong et al., 2019; Quass et al., 2024). Briefly, the average correlation of each matching pair of trials with the same stimulus is compared to a randomly sampled signal from the same trials 10000 times. The p-value is computed as the fraction of these randomly sampled signals with greater signal autocorrelation than the real data. P-values were then corrected for multiple comparisons using the Bonferroni-Holm method.

To identify clusters of ROIs characterized by being excited or inhibited by sound presentation, we performed a non-linear dimensionality reduction (t-SNE, Maaten and Hinton, 2008) using the average response over all angles/ROI for all significantly sound-responsive ROIs as input. Perplexity was determined empirically and finally defined as number of ROIs/10. Clustering was then performed to separate sound-excited from sound-inhibited ROIs using k-means (100 iterations (Hartigan and Wong, 1979) with nClusters being thus set to 2. Further population data analyses were thus based on either maxima or minima of Ca^{2+} responses averaged over each sound presentation angle.

For each ROI, the mean positive and negative ΔF/F peak at each presented angle was used to calculate orientation selectivity in sound-excited and inhibited ROIs, respectively. The orientation selectivity index was calculated as

$$\frac{R^{pref} - \emptyset R^{nonpref}}{R^{pref} + \emptyset R^{nonpref}},$$

where R^{pref} is the maximum/minimum response (peak ΔF/F) at the most preferred angle and $\emptyset R^{nonpref}$ is the average response at all other positions.

To track the activity of neurons across sessions of normal and altered binaural cues, ROIs of both FOVs (pre and post condition) were registered using a probabilistic, automated approach that quantitatively evaluates registration accuracy (CellReg, Sheintuch et al., 2017). Registration accuracy was re-evaluated manually and compared, resulting in a higher accuracy in the automated approach.

The support vector machine (SVM) classifier was used as a simple population analysis method to decode sound presentation angles based on the ΔF/F traces. The SVM was generated in MATLAB using the classification learner app, with “templateSVM” and "fitcecoc” as the main functions. A linear kernel and the sequential minimal optimization algorithm were used to build the classifier. The individual predictors were the ROI’s, and the classes were the different sound presentation angles, using equal priors. The absolute peaks of the ΔF/F traces from sound onset to 1 s after sound offset were used as the input data. The classifier was constructed, trained, and tested on each individual session per animal (unmatched data), or trained on a composite of the pre-plug sessions from all animals and tested on the post-plug sessions (matched data). To determine the decoding accuracy per session, 5-fold validation was used (5 randomly sampled portions of 80% of trials were used as training data, and the remaining 5 times 20% as test data). The “Accuracy” is given as the mean decoding accuracy among those five folds, normalized to “Balanced Accuracy” to account for an imbalanced number of trials per angle in the matched condition. Balanced Accuracy is defined as the mean of the micro-recalls (sensitivity or completeness, the number of true positives divided by the number of true positives and false negatives per angle), and its chance level is 1 divided by the number of angles. The “Shuffled” and “Shuffled Balanced” Accuracies were

computed by shuffling the trials and the class labels prior to classifier training and are used as a real chance level indicator.

Results

We virally expressed a genetically encoded calcium indicator (GCaMP6f or 8s; n = 2 and 7 mice, respectively) in the left IC of adult mice, and measured IC neuron sound responses under awake, head-fixed conditions using 2-photon Ca^{2+} imaging (Figure 1A,B; see also Methods). We investigated spatial receptive fields by developing a servo motor-based system that rotates a free-field speaker 180° in the horizontal frontal field around the mouse's head. This approach enabled us to present broadband noise bursts (4-35 kHz bandwidth; 500 ms duration) from one of seven distinct positions separated by 30 degrees on a trial-by-trial basis (Figure 1C). Of note, all analyses and figures represent positive and negative angles corresponding to speaker positions contra- and ipsi-lateral to the imaged IC respectively, with zero being centered on the midline.

Sound-inhibited neurons are less spatially selective than sound-excited neurons

Imaging data collection was restricted to fields of view (FOVs) 30-100 μm from the tectal surface in order to selectively study neurons of the higher-order "shell" IC layers (Figure 1D,E). We recorded from n = 2915 regions of interest (ROIs) corresponding to individual neuron somata (n = 34 FOVs in N = 9 mice), and quantified activity as the fluorescence intensity over time (ΔF/F) relative to a 1 s baseline period prior to sound presentation. Of those ROI's, 56.02 % (n = 1633/2915 neurons) were classified as significantly sound-modulated via an autocorrelation bootstrap analysis, and used for subsequent analyses (Geis et al., 2011; Wong and Borst, 2019; Quass et al., 2024, see Methods).

As a first pass characterization of spatial tuning, we performed t-SNE analysis in combination with k-means clustering based on each sound-responsive neuron's fluorescence waveform averaged across all sound presentation angles. This approach identified two clusters of sound-responsive neurons: 55.2% of neurons (n = 901/1633) showed reliable fluorescence increases and thus elevated their firing rates during

sound presentation and/or following sound offset (Figure 1F, orange trace). By contrast, the other 44.8% of neurons (n = 732/1633) reliably decreased their baseline fluorescence during sound presentation, and thus were sound-inhibited (Figure 1F, teal trace). These results indicate that in addition to sound-excited neuronal populations typically encountered in classic micro-electrode studies, nearly half of shell IC neurons are reliably inhibited by a given sound stimulus; these proportions are similar to recent reports using large scale recordings in the shell IC (Wong and Borst, 2019; Quass et al., 2024; Shi et al., 2024).

Sound presentation caused a bi-directional modulation of shell IC neuron fluorescence. Do excitation and inhibition show differential spatial selectivity? We addressed this question by averaging each neuron's fluorescence traces separately for every sound presentation angle. Whereas sound-excited neurons often showed preferential responses at particular spatial locations, the fluorescence decreases of sound inhibited neurons were often of similar magnitude regardless of presentation angle (Figure 1G,H; example neurons of each, indicated in Figure 1E). To compare the degree of spatial tuning across each group, we quantified the absolute maximum (sound-excited) or minimum (sound-inhibited) $\Delta F/F$ at each spatial position for sound-excited and sound-inhibited neurons respectively and calculated an orientation selectivity index (OSI) similar to previous studies (Zhao et al., 2013, see also Methods). The OSI standardizes neuronal response selectivity to a given set of stimuli between 0 and 1, with OSI = 0 reflecting equal responses to all sound presentation angles and OSI = 1 denoting a selective response to a single sound source location. Although the distributions of OSI values in both groups were broad, sound excited neurons had significantly higher OSI values and thus were more spatially selective than sound inhibited neurons (Figure 1I; Mann Whitney, $U = 41748$, $z = 15.3525$ $p < 0.0001$). These results suggest that postsynaptic targets of shell IC neurons may preferentially read out the representation of sound source location from increases, rather than decreases in neuronal firing rates.

Preferred spatial positions are not exclusive to the contralateral hemifield

Previous studies in the central IC report that neurons are strongly selective for contralateral sounds under binaural conditions (Middlebrooks, 1987; Park and Pollak, 1993; Klug et al., 1995, 1999b; Day and

Delgutte, 2013; Yao et al., 2013; Grothe and Pecka, 2014) with minimal responses in the ipsilateral hemifield. However, both sound-excited and sound-inhibited neurons in our datasets changed their firing rates when sounds were presented in both ipsi- and contra-lateral hemifields, suggesting that shell IC populations represent the entire frontal azimuth. Accordingly, the preferred angles of sound-excited neurons were not exclusively contralateral: Some neurons were monotonically responsive to sounds in the ipsilateral hemifield (Figure 2A), whereas others had spatial receptive fields preferring intermediate positions such as the midline (Figure 2B). These observations are reminiscent of spatial tuning reported in barn owl external IC (Knudsen and Konishi, 1980), IC brachium (Schnupp and King, 1997; Slee and Young, 2014) and superior colliculus (King and Hutchings, 1987; King et al., 1998; Ito et al., 2020). As such, the distribution of preferred angles in sound excited neurons tiled both ipsi- and contralateral hemifields. A qualitatively similar distribution was observed in the sound inhibited neuron population (Figure 2C,D), which is perhaps not surprising given the broad spatial responsiveness of sound-evoked fluorescence decreases (Figure 1G-I). Taken together, the distribution of preferred angles for all neurons (Fig 2D) was not significantly different between hemifields (χ^2 (1) = 2.9244, p = 0.0872). Thus, in contrast to the largely monotonic, contralateral representation of auditory space found in central IC, shell IC neurons in a single hemisphere represent the entire frontal azimuth via monotonic and non-monotonic tuning.

Two groups of sound-excited neurons transmit distinct population-level azimuth representations

Given the above tuning diversity, we next asked if sound excited and sound inhibited shell IC neuron populations could be further subdivided into functionally meaningful clusters that transmit specialized spatial information. To this end, we incrementally sub-clustered response shapes of sound-excited and sound-inhibited neurons using t-SNE and k-means clustering of the fluorescence waveforms averaged across all presentation angles. Whereas this approach failed to yield visibly meaningful sub-clusters among the sound-inhibited neurons (data not shown), sound-excited neurons sub-clustered into one of two groups with distinct activity profiles. In the first group, most neurons showed a single rising phase of fluorescence increase that typically occurred during sound presentation (Figure 3A; n = 350/901, or

389 38.8%). Interestingly, the distribution of preferred angles in these “group 1” neurons showed a clear and
390 significant contralateral bias, although substantial ipsilateral responses were nevertheless apparent
391 (Figure 3B,C, $\chi^2(1) = 63.7120$, $p = 1.4400e^{-15}$). Most neurons in the second group showed a bi-directional
392 response profile: A brief inhibitory ON response during sound presentation followed by a sharp excitatory
393 OFF response upon sound termination (Figure 3D; n = 551/901, or 61.2%). In contrast to the contralateral
394 bias of group 1 neurons, the distributions of preferred angles for the sound excited OFF responses were
395 significantly biased towards the ipsilateral side (Figure 3E-F, $\chi^2(1) = 17.6347$, $p = 2.6766e^{-05}$). The
396 distribution of the preferred angles for the negative ON response however were largely uniform across
397 the frontal azimuth (Figure 3G-H, $\chi^2(1) = 0.6280$, $p = 0.4281$). In addition to these differences between
398 ipsilateral and contralateral distributions within individual data sets, a difference between distributions of
399 preferred peaks across sound presentation angles could be observed (group 1 vs. OFF responses of
400 group 2, 2-sample χ^2-test, χ^2 (7) = 49.114, $p = 2.1552e^{-08}$). When comparing degree of spatial tuning
401 across data sets, distributions of OSI values differed significantly across group 1 neurons and the
402 inhibitory ON response of group 2 neurons, but not between positive components of both groups (data
403 not shown, Kruskal-Wallis test, χ^2 (2) = 6.957, p = 0.0309, group 1 vs. group 2 ON; Dunn’s multiple
404 comparison, p = 0.0283). Altogether these data suggest that shell IC neurons in a single hemisphere
405 represent the onset and termination of sounds emanating across the entire frontal azimuth via firing rate
406 increases. However, distinct temporal characteristics appear to be segregated to largely non-overlapping
407 neuronal populations which differentially contribute ipsi- vs contralateral signals.
408
409 In the auditory brainstem, excitatory OFF responses can be generated by rebound firing following the
410 offset of sound-evoked, hyperpolarizing inhibition (Kopp-Scheinpflug et al., 2011). Are OFF responses in
411 group 2 neurons due to rebound firing upon the cessation of sound-evoked inhibition? If true, the
412 characteristics of the inhibitory ON and excitatory OFF responses should correlate in single neurons.
413 However, OSI values were not significantly correlated (Figure 3I; Pearson, r(549) = 0.6271, p = 0.1415,
414 $R^2 = 0.004$). These data argue that the selectivity of OFF excitation does not arise due to rebound firing

upon cessation of sound-evoked inhibition, but rather that temporally separate phases of activity may originate via distinct sets of synapses impinging upon the same neuron (Scholl et al., 2010).

Differentially tuned ON and OFF excitation converges onto single neurons

We also observed a minor fraction of sound-excited neurons in our datasets with ON and OFF excitatory responses. These dual ON-OFF excited neurons were found in both group 1 and 2 defined by our t-SNE clustering of Figure 3; the lack of separation from the larger two populations likely reflects the relative paucity of this response type as well as a limitation of our clustering methods. Interestingly, the spatial receptive fields of ON and OFF responses were often not congruous (Figure 4A; n = 33 neurons from N = 8 mice). Importantly, the differential spatial tuning of ON and OFF excitation was not an artifact of GCaMP saturation during the ON response at preferred angles: The within-cell difference in preferred angles for ON and OFF responses was also apparent in the rate-of-rise, instead of the peak, of the fluorescence traces (Figure 4B). The distribution of preferred angles for ON responses showed an over-representation of contralateral positions whereas preferred angles of OFF responses were more evenly distributed across the entire frontal hemifield (Kolmogorov-Smirnoff-Test - D = 0.3235, p = 0.044). Within-cell comparisons revealed that absolute difference in preferred angles for ON and OFF responses was separated by >60 degrees in 28/33 neurons, and significantly different from a hypothetical median of zero (Figure 4D, one sample Wilcoxon test, z = 4.9746, p = $6.538e^{-7}$). By contrast, OSI values were similar for excitatory ON and excitatory OFF fluorescence peaks (Figure 4E, Wilcoxon signed-rank test, z = -0.16974, p = 0.86521). Altogether these analyses further support the idea that ON and OFF spatial receptive fields reflect activity at non-overlapping sets of synapses.

Monaural ear plugging has diverse effects on single neuron receptive fields

Sounds presented at the ipsilateral ear strongly reduce IC neuron spiking (Rose et al., 1966; Wenstrup et al., 1988; Irvine and Gago, 1990; Delgutte et al., 1999; Xiong et al., 2013; Ono and Oliver, 2014) and this phenomenon is thought to contribute to interaural level difference (ILD) coding and contralateral dominance of spatial selectivity for suprathreshold sounds in the IC (Li et al., 2010; Li and Pollak, 2013).

Indeed, acute or chronic monaural ear plugging drastically broadens the spatial receptive fields of IC neurons and their downstream targets (Middlebrooks, 1987; Park and Pollak, 1993; Klug et al., 1995, 1999b; Day and Delgutte, 2013; Grothe and Pecka, 2014). Given the diversity of ipsi- and contralateral spatial selectivity in dorsal shell IC neurons (Figures 1 and 2), to what extent do ipsilateral sounds contribute to the spatial selectivity and population-level representations of auditory space? We addressed this question by measuring the acoustic responses of the *same* dorsal shell IC neurons before and immediately after monaural plugging of the ipsilateral ear (Figure 5A,B. N = 6 mice; see Methods). This manipulation caused an average of ~45-55 dB SPL threshold shifts for all frequencies tested at the plugged ear, as confirmed using pure-tone auditory brainstem response measurements (N = 3 mice).

We used an offline approach to track individual neurons and perform within-cell comparisons of spatial sound responses across pre- and post-plug sessions (Sheintuch et al., 2017, see Methods). Monaural ear plugging exerted diverse effects in individual shell IC neurons. In 52 neurons (42%), ear-plugging broadened spatial receptive fields, reduced OSI, and degraded spatial selectivity (Figure 5C,D). These observations agree with prior studies showing that ipsilateral sounds have a net inhibitory effect on some IC neuron sound responses (Kuwada et al., 1997; Sanes et al., 1998; Breebaart et al., 2001; Ono and Oliver, 2014). In other neurons however, ear plugging instead increased sound responses and sharpened OSI values compared to pre-plug conditions. Indeed, 8 neurons that were minimally responsive or sound inhibited in the pre-plug condition became sound-excited following ear plugging with clearly defined spatial receptive fields (Figure 5E). Before ear-plugging, preferred angles of sound responsive neurons tracked across both conditions (n = 124 from N = 6 mice) equally tiled the entire frontal hemifield (Figure 5F, $X^2(1) = 0.0164$, $p = 0.898$). This distribution is like that of the larger population of neurons recorded in pre-plug conditions (e.g., Figure 2D). In post-plug sessions, the distribution of preferred angles shifted towards the ipsilateral hemifield (Figure 5F, $X^2(1) = 10.5491$, $p = 0.0012$), despite an increased sound attenuation at the ipsilateral ear. Interestingly, ear-plugging did not reduce the relative orientation selectivity of sound responsive neurons (Figure 5G, relative difference between pre- and post-plugged OSI, Wilcoxon signed rank, $z = 1.6526$, $p = 0.2602$). Rather, robust spatial tuning appeared to originate

from different neuronal sub-populations in pre- and post-plugged conditions: 42 % of ROIs decreased, while 58 % increased OSI values following ear-plugging, such that the *absolute* change in OSI values was significantly different across pre- and post-plug conditions (Figure 5G, absolute difference between pre- and post-plugged OSI, Wilcoxon signed rank, $z = 7.9135$, $p = 0.001$). Thus, ipsilateral ear-plugging substantially impacts spatial sound responses by shifting the spatial selectivity (Figure 5C,D) and even the response directionality (Figure 5E) of individual shell IC neurons. However, the entire frontal azimuth was nevertheless represented by the distribution of preferred angles of single neurons, and relative OSI values were unchanged.

Population coding of auditory space persists despite monaural conductive hearing loss

The above observations suggest that ipsilateral ear plugging degrades spatial selectivity in some neurons, while unmasking spatial sound responses in previously non-selective neurons. Consequently, conductive hearing loss may result in a “remapping” of shell IC population codes, such that spatially selective neural population activity could persist despite significant and abrupt changes in binaural cue availability. To further understand how shell IC neuron populations transmit spatial information under altered binaural conditions, we analyzed pre- and post-plug imaging sessions without explicitly tracking neurons across the two conditions. We first asked if ipsilateral ear plugging impacts the percentage of sound responsive neurons in the shell IC. To this end we employed the bootstrapping autocorrelation procedure to determine response reliability of neurons at specific sound presentation angles (Geis et al., 2011; Wong & Borst, 2019). 238/437 ROIs (54%) in n = 6 pre-plug FOVs from N = 6 mice were significantly sound responsive to at least one presentation angle, and a similar percentage of sound-responsive neurons was observed in post-plug FOVs (Figure 6A; 236/441, 54%).

Additionally, the relative proportions of sound excited and inhibited neurons remained similar across pre- and post-plug conditions (Figure 6A, $\chi^2(1) = 0.2964$, $p = 0.5862$). Pre-plugging, the distribution of preferred angles tiled the entire frontal hemifield (Figure 6A, $\chi^2(1) = 0.3124$, $p = 0.5762$) whereas the population was modestly skewed towards ipsilateral preferred angles in the post-plug condition (Figure

6A,B, $\chi^2(1) = 10.5491$, $p = 0.0012$). Moreover, ipsilateral ear-plugging did not impact the overall resolution of spatial receptive fields, as OSI of sound-excited and sound-inhibited neurons were similar in pre- and post-plug imaging sessions (Figure 6C; Kruskal-Wallis $H(3) = 126.6$, $p < 0.05$, effect size ($\eta 2$) = 0.016; Dunn's post hoc comparison: pre-plug excited vs pre-plug inhibited, $p < 0.001$; post-plug excited vs post-plug inhibited, $p < 0.001$); these results mirror our within-neuron comparisons (Figure 5). As the population-level spatial tuning persisted in both pre- and post-plug sessions, these results argue that dorsal shell IC neurons can transmit spatial information upon reduced binaural cue availability. In summary, ipsilateral ear plugging does not reduce the percentage of shell IC neurons transmitting spatial information under our conditions. Rather, it shifts the distribution of preferred angles without altering the overall acuity of receptive fields. Thus, an altered, but nevertheless observable, population-level representation of the frontal azimuth remains following ipsilateral occlusion.

Representational drift does not account for effects of ear-plugging on shell IC spatial tuning

Pre- and post-plug imaging data were collected ~5-6 hours apart, such that any "representational drift" (Rule et al., 2019; Deitch et al., 2021; Aitken et al., 2022) of spatial sound responses would be unlikely account for the results of Figures 5 and 6. However, to determine the extent to which the above results are due to ear-plugging, we imaged n = 4 FOVs from N = 2 mice undergoing the same anesthesia protocol as for the 6 experimental mice but without fitting an earplug (Figure 7A,B). Although we observed shifts in OSI values and preferred positions in both groups, the median ΔOSI values were significantly lower for sham (0.0532 ± 0.0382, median ± median absolute deviation) and experimental mice (0.093 ± 0.0597, median ± median absolute deviation, Wilcoxon ranksum-test: $W = 19272$, $z = 3.9801$, $p = 0.000068892$). Additionally, the extent of lateral jitter - Δ angle of the peak response given in degrees – 7C - was significantly less in sham compared to experimental mice (Kolmogorov-Smirnoff-Test - $D = 0.2471$, $p = 0.0004$). However, the Δ angle did not predict Δ OSI in either dataset (Figure 7D; linear regression - experiment: $F(1,123) = 0.020208$, $p = 0.88716$, sham: $F(1,144) = 1.8839$, $p = 0.172$), suggesting that the extent of changes in OSI values did not simply reflect differences in lateral jitter between sham and experimental groups. Finally, we correlated tuning curves in the pre and the post condition for both

experimental and sham data (Figure 7E): tuning curves corelated significantly less in the actual experiment than in the sham treatment (Kolmogorov-Smirnoff-Test - D = 0.2079 , p = 0.0062). Taken together, our results demonstrate that monaural conductive hearing loss, rather than effects of anesthesia or representational drift, alters dorsal shell IC neuron spatial sound responses. Moreover, the smaller overall shifts in spatial tuning in sham mice may reflect a combination of broad spatial tuning and trial-to-trial variability in shell IC sound responses. Alternatively, uncontrolled differences between sham and experimental groups such as differences in pinnae movements could also contribute.

Sound presentation angle can be decoded via neural data recorded in monaurally occluded mice

If dorsal shell IC populations effectively transmit auditory spatial information under binaural conditions and after ear plugging, neural population data recorded in either condition should be similarly informative of sound source location. To test this hypothesis, we asked if support vector machine (SVM) classifiers could decode the sound presentation angle when trained on fluorescence data recorded from either pre- or post ear-plug sessions (Figure 8A). SVMs trained on pre-plugging sessions classified sound presentation angle significantly above chance level when tested on held out trials from the same pre-plug sessions (median accuracy: 39.4 %, 24.5 % above chance level obtained from shuffled data, Figure 8B, golden box, Bonferroni, pre-plugged vs. chance = $p < 0.001$). This result argues that shell IC neuron populations provide downstream brain regions with substantial information regarding sound source location. Interestingly, SVMs trained and tested on the post-plugging data could also correctly classify the trial-by-trial sound presentation angle significantly above chance level (median accuracy: 33.9 %, 19.3 % above chance level, Figure 8B, teal box, Bonferroni, post-plugged vs chance = $p < 0.001$), and this performance was not significantly different from the classification accuracy of SVMs trained and tested on the pre-plug sessions (Bonferroni test, pre-plugged vs post-plugged = n.s., $p > 0.05$). This result further supports the interpretation that subsets of the shell IC population can transmit spatial acoustic information despite altered binaural cues.

549 To further test if distinct groups of shell IC neurons transmit directional information under binaural and
550 monaural conditions, we trained SVM classifiers on neural activity recorded in pre-plugging sessions and
551 measured their classification accuracy on trials from post-plugging sessions. For these analyses, data
552 were pooled for all mice to increase the number of trackable neurons, and only matched sound-
553 responsive ROI's were included as in figure 7. SVMs were then trained on an ensemble population
554 created from all animals. Accordingly, SVMs trained on pre-plugging data displayed 23.6% accuracy
555 (merely 6.1% above chance level) when classifying sound source location from neural activity of the
556 same neurons recorded in post-plugging sessions (Figure 8C, teal box). This result was not due to a lack
557 of directional information in the training datasets: SVMs trained on the same pre-plugging datasets
558 reached a median accuracy of 46.5% when tasked with classifying pre-plugging trials held out from the
559 training data (Figure 8C, golden box). Additionally, the results were unlikely caused by overfitting, as
560 removing a randomly chosen subpopulation of neurons in each trial still resulted in sound angle decoding
561 accuracy significantly above chance level (Figure 8D). Moreover, SVMs trained on pre- or post-sham
562 treatment imaging data showed high classification accuracy when tested on held out trials from within
563 the same session (e.g., pre- or post-sham trained/tested; Figure 8E), as well as across sessions (pre-
564 sham trained/post-sham tested, Figure 8F). These results rule out the interpretation that SVMs trained
565 on pre-plug data fail to accurately classify post-plugging trials due to a non-specific effects of anesthesia
566 or representational drift. Rather, in tandem with the results of figures 5 and 6, our data suggest that
567 distinct shell IC population codes transmit directional information under binaural and monaural hearing
568 conditions.
569
570 **Decoding errors reflect misclassification of ipsilateral angles**
571 As reported above, decoding accuracy is reduced when the classifier is trained on pre- and tested on
572 post-plug data. We further probed the mechanism underlying this effect by comparing the distribution and
573 magnitude of incorrect classifications for SVMs trained on pre-plug datasets and tasked to classify post-
574 plug responses from the same neurons. Monaural ear plugging introduces a strong bias towards the
575 unplugged side: on incorrect classifications, the classifier is much more likely to classify a sound to be

presented from the right (unplugged) side (Figure 9A, Trained Pre / Tested Post: χ^2 (1) = 505.0485, p = $7.5774e^{-112}$, n = 1030, median error = +30°). In contrast, SVMs trained on data from sham treated mice showed a much more symmetric prediction error histogram, with ipsi and contralateral errors equally distributed around 0 (Figure. 9B Trained Pre / Tested Post: χ^2 (1) = 582.4242, p = $1.1137e^{-128}$, n = 1320, median error = +15°). Qualitatively similar results are seen when comparing the confusion matrices for the two classifier types: Whereas SVMs trained and tested on pre-plug datasets rarely classified ipsilateral sounds as arising from contralateral angles (experimental data: χ^2 (1) = 38,3789, p = $5.826e^{-10}$, n = 908, median error = 0°; sham data: χ^2 (1) = 582.4242, p = $1.1137e^{-128}$, n = 1320, median error = +15°) pre-plug trained SVMs showed a strong contralateral (open ear) bias for all angles when tested on post-plug data (Figure 9C). Intermediate ipsilateral angles and the midline were almost always misclassified as originating from the contralateral hemifield. These results were not observed in confusion matrices from sham treated mice (Figure 9D). Rather, our population coding data are reminiscent of psychophysical performance errors, whereby acute monaural deprivation induces a strong perceptual bias for sounds originating from the open ear (Florentine, 1976b; Slattery III and Middlebrooks, 1994; Kumpik et al., 2010; Keating et al., 2016).

Discussion

We have shown that activity of neurons in the IC's superficial "shell" layers represent the entirety of the frontal azimuth, even when binaural cues are abruptly and dramatically altered by monaural conductive hearing loss. Our results contrast somewhat with single unit studies of binaural responses in the IC's lemniscal central nucleus, where contralateral excitation and ipsilateral inhibition often give rise to a dominance of contralateral selectivity, and a largely monotonic coding of azimuthal lateralization in the central IC (Li et al., 2010; Li and Pollak, 2013; Xiong et al., 2013; Yao et al., 2013; van den Wildenberg and Bremen, 2024). Additionally, in contrast to the IC brachium (Schnupp and King, 1997; Slee and Young, 2013, 2014) and superior colliculus (King and Hutchings, 1987; Ito et al., 2020), which report predominantly contralateral representation of auditory space under binaural conditions, we find that almost half of dorsal shell IC neurons (42.38 %) showed dominant responses in the ipsilateral hemifield.

If central, brachial, and dorsal shell IC neurons project to divergent postsynaptic targets, the auditory midbrain could transmit parallel but complementary spatial auditory signals that may be involved in distinct behaviors (Brandão et al., 1993; Xiong et al., 2015; Hu and Dan, 2022). Future studies using sub-region specific optogenetic manipulations in behaving mice could directly test this idea.

Origin of spatial tuning diversity

One potential mechanism of ipsilateral tuning is the commissural projection of the IC. Accordingly, unilateral IC silencing impacts spatial tuning in the opposite IC (Orton et al., 2016; Liu et al., 2022), suggesting that reciprocal interactions between hemispheres govern IC neuron responses. Alternatively, ipsilateral responses could originate in part via auditory corticofugal projections that target dorsomedial IC neurons (Winer et al., 1998; Oberle et al., 2022, 2023): Indeed, single auditory cortical hemispheres contain neurons tuned to the entire azimuthal plane (Rajan et al., 1990; Panniello et al., 2018; Remington and Wang, 2019; Wood et al., 2019; Amaro et al., 2021) with many neurons showing circumscribed receptive fields as described here (Middlebrooks and Pettigrew, 1981). Additionally, silencing auditory cortex profoundly impacts IC neuron binaural receptive fields (Nakamoto et al., 2008). However, the complicated interconnectivity between IC and auditory cortex complicates disambiguating whether changes in receptive field properties upon silencing of synaptic input pathways reflect a loss-of-function of spatially tuned synaptic drive, or rather brain-wide network effects.

OFF responses exhibit spatial selectivity

In addition to spatially tuned activity during sound presentation, 551/901 (61.2 %) sound-excited neurons exhibited OFF responses upon sound termination, which were often spatially selective. At the population level, ON and OFF responses displayed similar distributions of preferred locations with similar OSI values. Although many OFF responsive neurons were also sound inhibited, sound-evoked inhibition was less selective for spatial position than sound-evoked excitation (Figure 2). Consequently, rebound firing following release of inhibition is unlikely to fully explain OFF responses. This interpretation is further supported by the observation of a handful of neurons (33/551 or 6%) showing both excitatory ON and

630 excitatory OFF responses with significantly distinct spatial receptive fields. Rather, these data suggest
631 that multiple, spatially selective synaptic inputs can converge upon single shell IC neurons. This result is
632 reminiscent of classic observations in primary visual cortex, showing that simple cells have ON and OFF
633 receptive fields which code for distinct spatial locations (Hubel and Wiesel, 1962). Together with prior
634 studies reporting spatially distinct ON and OFF receptive fields in auditory cortex (Hartley et al., 2011;
635 Ramamurthy and Recanzone, 2017), our results suggest that common organizational principles of spatio-
636 temporal processing exist across sensory systems.
637
638 **Population coding of spatial location persists with altered binaural cues**
639 Ipsilateral ear plugging broadens and shifts spatial receptive fields in single unit recordings from brain
640 regions of various species (Palmer and King, 1985; Gooler et al., 1996b; Grant and Binns, 2003b) though
641 some spatial selectivity persists in individual neurons (Middlebrooks, 1987; Samson et al., 2000; Poirier
642 et al., 2003). However, the extent to which such altered population-level activity could accurately transmit
643 spatial auditory information was unclear. In our studies, ipsilateral ear plugging did indeed broaden the
644 receptive fields in a subset of spatially tuned shell IC neurons. However, a substantial proportion (58%)
645 of neurons remained spatially selective or sharpened their spatial tuning, and ipsilateral ear plugging
646 unmasked spatial receptive fields in a subset of previously less selective neurons. The spatial receptive
647 fields which persist following ipsilateral ear plugging may reflect a selectivity to monaural spectral cues
648 or possibly a non-monotonic ,“O-shaped” level dependence of ipsilateral sounds (Davis et al., 1999).
649 Alternatively, de novo spatial tuning could also reflect a rapid (<2 hr) and experience independent
650 plasticity of binaural cues. In either case, the functional consequence is that ipsilateral ear plugging did
651 not degrade the population level spatial representations as predicted from single unit data, but rather
652 caused a functional reorganization of which neurons were spatially informative in normal vs. altered
653 binaural conditions. In support of this interpretation, simple classifier models trained and tested on
654 imaging data collected in either control or ipsilateral plugged conditions could predict sound presentation
655 angle with similar above chance accuracy, but classification accuracy dropped to near chance level when
656 classifiers were tested across conditions. Interestingly, models trained on control sessions and tested on

ear-plugged sessions exhibited classification errors reminiscent of human and animal behavior, whereby acute monaural hearing loss induces a perceptual bias towards the open ear (Slattery III and Middlebrooks, 1994; Sanchez Jimenez et al., 2023). However, future studies are required to establish the extent to which dorsal shell IC neuron activity causally relates to spatial auditory percepts.

Implications for spatial cue plasticity following monaural hearing loss

Humans and animals show profound impairments in sound localization immediately following monaural hearing loss. However, many studies show that they can eventually re-learn to localize sounds. This form of perceptual learning occurs both during the juvenile critical period and in adulthood (Moore et al., 1999), and is thought to require active training (Wilmington et al., 1994; Bajo et al., 2010, 2019) to remap altered binaural cues onto spatial locations and/or a re-weighting of the importance of monaural spectral cues (Hofman et al., 1998; Shinn-Cunningham, 2001; Kacelnik et al., 2006; Kumpik et al., 2019; Zonooz and Van Opstal, 2019). Although the biological mechanisms of this perceptual learning are unclear, circumstantial evidence implicates the dorsal shell IC as a potential locus of experience-dependent plasticity which could contribute to this perceptual learning. The external IC nucleus of the barn owl, which is thought analogous to the mammalian shell IC nuclei, is a major site of experience-dependent plasticity for spatial auditory representations (Gold and Knudsen, 2000). Interestingly, the spatial receptive fields acquired via experience do not “overwrite” pre-existing spatial representations, but rather suppress their expression via GABAergic inhibition. Consequently, multiple spatial population codes can co-exist in the same IC tissue and be recalled in a context-dependent manner (Zheng and Knudsen, 1999). Under our conditions, a population representation of auditory space emerged rapidly in the mammalian shell IC following monaural ear plugging, albeit in a seemingly experience-independent manner. However, this phenomenon may nevertheless reflect the similar principle of context-dependent expression of spatial population codes as reported in owls. In this framework, the re-learning of sound localization following monaural hearing loss might thus involve plasticity mechanisms in shell IC neurons’ downstream targets “learning” to use a newly informative spatial auditory population code.

References

Aitken K, Garrett M, Olsen S, Mihalas S (2022) The geometry of representational drift in natural and artificial neural networks Latham PE, ed. PLOS Comput Biol 18:e1010716.

Amaro D, Ferreiro DN, Grothe B, Pecka M (2021b) Source identity shapes spatial preference in primary auditory cortex during active navigation. Curr Biol 31:3875-3883.e5.

Baguley DM., Bird J, Humphriss R L, Prevost AT (2006) The evidence base for the application of contralateral bone anchored hearing aids in acquired unilateral sensorineural hearing loss in adults. Clin Otolaryngol 31:6–14.

Bajo VM, Nodal FR, Korn C, Constantinescu AO, Mann EO, Boyden ES, King AJ (2019) Silencing cortical activity during sound-localization training impairs auditory perceptual learning. Nat Commun 10:3075.

Bajo VM, Nodal FR, Moore DR, King AJ (2010) The descending corticocollicular pathway mediates learning-induced auditory plasticity. Nat Neurosci 13:253–260.

Barsy B, Kocsis K, Magyar A, Babiczky Á, Szabó M, Veres JM, Hillier D, Ulbert I, Yizhar O, Mátyás F (2020) Associative and plastic thalamic signaling to the lateral amygdala controls fear behavior. Nat Neurosci 23:625–637.

Bauer RW, Matuzsa JL, Blackmer RF, Glucksberg S (1966) Noise Localization after Unilateral Attenuation. J Acoust Soc Am 40:441–444.

Bergan JF, Ro P, Ro D, Knudsen EI (2005) Hunting Increases Adaptive Auditory Map Plasticity in Adult Barn Owls. J Neurosci 25:9816–9820.

Brainard M, Knudsen E (1993) Experience-dependent plasticity in the inferior colliculus: a site for visual calibration of the neural representation of auditory space in the barn owl. J Neurosci 13:4589–4608.

Brandão ML, Melo LL, Cardoso SH (1993) Mechanisms of defense in the inferior colliculus. Behav Brain Res 58:49–55.

Breebaart J, Van De Par S, Kohlrausch A (2001) Binaural processing model based on contralateral inhibition. I. Model structure. J Acoust Soc Am 110:1074–1088.

Burger RM, Pollak GD (2001) Reversible Inactivation of the Dorsal Nucleus of the Lateral Lemniscus Reveals Its Role in the Processing of Multiple Sound Sources in the Inferior Colliculus of Bats. J Neurosci 21:4830–4843.

Cai D, Yue Y, Su X, Liu M, Wang Y, You L, Xie F, Deng F, Chen F, Luo M, Yuan K (2019) Distinct Anatomical Connectivity Patterns Differentiate Subdivisions of the Nonlemniscal Auditory Thalamus in Mice. Cereb Cortex 29:2437–2454.

Cassinotti LR, Ji L, Borges BC, Cass ND, Desai AS, Kohrman DC, Liberman MC, Corfas G (2022) Cochlear Neurotrophin-3 overexpression at mid-life prevents age-related inner hair cell synaptopathy and slows age-related hearing loss. Aging Cell 21:e13708.

721 Champoux F, Paiement P, Mercier C, Lepore F, Lassonde M, Gagné JP. (2007) Auditory processing in
722 a patient with a unilateral lesion of the inferior colliculus. Eur J Neurosci 25:291–297.

723 Chen C, Cheng M, Ito T, Song S (2018) Neuronal Organization in the Inferior Colliculus Revisited with
724 Cell-Type-Dependent Monosynaptic Tracing. J Neurosci 38:3318–3332.

725 Davis KA, Ramachandran R, May BJ (1999) Single-Unit Responses in the Inferior Colliculus of
726 Decerebrate Cats II. Sensitivity to Interaural Level Differences. J Neurophysiol 82:164–175.

727 Day ML, Delgutte B (2013) Decoding Sound Source Location and Separation Using Neural Population
728 Activity Patterns. J Neurosci 33:15837–15847.

729 Deitch D, Rubin A, Ziv Y (2021) Representational drift in the mouse visual cortex. Curr Biol 31:4327-
730 4339.e6.

731 Delgutte B, Joris PX, Litovsky RY, Yin TCT (1999) Receptive Fields and Binaural Interactions for
732 Virtual-Space Stimuli in the Cat Inferior Colliculus. J Neurophysiol 81:2833–2851.

733 Firszt JB, Reeder RM, Dwyer NY, Burton H, Holden LK (2015) Localization training results in
734 individuals with unilateral severe to profound hearing loss. Hear Res 319:48–55.

735 Fitzpatrick DC, Batra R, Stanford TR, Kuwada S (1997) A neuronal population code for sound
736 localization. Nature 388:871–874.

737 Florentine M (1976a) Relation between lateralization and loudness in asymmetrical hearing losses. J
738 Am Audiol Soc 1:243–251.

739 Florentine M (1976b) Relation between lateralization and loudness in asymmetrical hearing losses. J
740 Am Audiol Soc 1:243–251.

741 Geis H -Rüdiger AP, Van Der Heijden M, Borst JGG (2011) Subcortical input heterogeneity in the
742 mouse inferior colliculus. J Physiol 589:3955–3967.

743 Gleiss H, Encke J, Lingner A, Jennings TR, Brosel S, Kunz L, Grothe B, Pecka M (2019) Cooperative
744 population coding facilitates efficient sound-source separability by adaptation to input statistics
745 Bizley JK, ed. PLOS Biol 17:e3000150.

746 Gold JI, Knudsen EI (1999) Hearing Impairment Induces Frequency-Specific Adjustments in Auditory
747 Spatial Tuning in the Optic Tectum of Young Owls. J Neurophysiol 82:2197–2209.

748 Gold JI, Knudsen EI (2000) A Site of Auditory Experience-Dependent Plasticity in the Neural
749 Representation of Auditory Space in the Barn Owl's Inferior Colliculus. J Neurosci 20:3469–
750 3486.

751 Gooler DM, Xu J, Feng AS (1996a) Binaural inhibition is important in shaping the free-field frequency
752 selectivity of single neurons in the inferior colliculus. J Neurophysiol 76:2580–2594.

753 Gooler DM, Xu J, Feng AS (1996b) Binaural inhibition is important in shaping the free-field frequency
754 selectivity of single neurons in the inferior colliculus. J Neurophysiol 76:2580–2594.

755 Goyer D, Silveira MA, George AP, Beebe NL, Edelbrock RM, Malinski PT, Schofield BR, Roberts MT
756 (2019) A novel class of inferior colliculus principal neurons labeled in vasoactive intestinal
757 peptide-Cre mice. eLife 8:e43770.

758 Grant S, Binns KE (2003a) Reduced influence of the ipsilateral ear on spatial tuning of auditory neurons
759 in the albino superior colliculus: a knock-on effect of anomalies of the acoustic chiasm? Exp
760 Brain Res 151:478–488.

761 Grant S, Binns KE (2003b) Reduced influence of the ipsilateral ear on spatial tuning of auditory neurons
762 in the albino superior colliculus: a knock-on effect of anomalies of the acoustic chiasm? Exp
763 Brain Res 151:478–488.

764 Grothe B and Pecka M (2014) The natural history of sound localization in mammals – a story of
765 neuronal inhibition. *Front. Neural Circuits* **8**:116.

766 Grothe B, Pecka M, McAlpine D (2010) Mechanisms of Sound Localization in Mammals. Physiol Rev
767 90:983–1012.

768 Hartigan JA, Wong MA (1979) Algorithm AS 136: A K-Means Clustering Algorithm. J R Stat Soc Ser C
769 Appl Stat 28:100–108.

770 Hartley DEH, Dahmen JC, King AJ, Schnupp JWH (2011) Binaural sensitivity changes between cortical
771 on and off responses. J Neurophysiol 106:30–43.

772 Hine JE, Martin RL, Moore DR (1994) Free-field binaural unmasking in ferrets. Behav Neurosci
773 108:196–205.

774 Hofman PM, Van Riswick, Jos G A, Van Opstal, A John (1998) Relearning sound localization with new
775 ears. Nat Neurosci 1:5.

776 Hoy JL, Yavorska I, Wehr M, Niell CM (2016) Vision Drives Accurate Approach Behavior during Prey
777 Capture in Laboratory Mice. Curr Biol 26:3046–3052.

778 Hu F, Dan Y (2022) An inferior-superior colliculus circuit controls auditory cue-directed visual spatial
779 attention. Neuron 110:109-119.e3.

780 Hubel DH, Wiesel TN (1962) Receptive fields, binocular interaction and functional architecture in the
781 cat's visual cortex. J Physiol 160:106–154.

782 Irvine DR, Gago G (1990) Binaural interaction in high-frequency neurons in inferior colliculus of the cat:
783 effects of variations in sound pressure level on sensitivity to interaural intensity differences. J
784 Neurophysiol 63:570–591.

785 Ito S, Si Y, Feldheim DA, Litke AM (2020) Spectral cues are necessary to encode azimuthal auditory
786 space in the mouse superior colliculus. Nat Commun 11:1087.

787 Jenkins WM, Masterton RB (1982) Sound localization: effects of unilateral lesions in central auditory
788 system. J Neurophysiol 47:987–1016.

789 Kacelnik O, Nodal FR, Parsons CH, King AJ (2006) Training-Induced Plasticity of Auditory Localization
790 in Adult Mammals Shamma S, ed. PLoS Biol 4:e71.

791 Keating P, Dahmen JC, King AJ (2013) Context-Specific Reweighting of Auditory Spatial Cues
792 following Altered Experience during Development. Curr Biol 23:1291–1299.

793 Keating P, Rosenior-Patten O, Dahmen JC, Bell O, King AJ (2016) Behavioral training promotes
794 multiple adaptive processes following acute hearing loss Mrsic-Flogel TD, ed. eLife 5:e12264.

King AJ, Hutchings ME (1987) Spatial response properties of acoustically responsive neurons in the superior colliculus of the ferret: a map of auditory space. J Neurophysiol 57:596–624.

King AJ, Jiang ZD, Moore DR (1998) Auditory brainstem projections to the ferret superior colliculus: anatomical contribution to the neural coding of sound azimuth. J Comp Neurol 390:342–365.

Kira S, Safaai H, Morcos AS, Panzeri S, Harvey CD (2023) A distributed and efficient population code of mixed selectivity neurons for flexible navigation decisions. Nat Commun 14:2121.

Klug A, Bauer EE, Pollak GD (1999) Multiple Components of Ipsilaterally Evoked Inhibition in the Inferior Colliculus. J Neurophysiol 82:593–610.

Klug A, Park TJ, Pollak GD (1995) Glycine and GABA influence binaural processing in the inferior colliculus of the mustache bat. J Neurophysiol 74:1701–1713.

Knudsen EI, Esterly SD, Knudsen PF (1984a) Monaural occlusion alters sound localization during a sensitive period in the barn owl. J Neurosci 4:1001–1011.

Knudsen EI (2004) Sensitive Periods in the Development of the Brain and Behavior. J Cogn Neurosci 16:1412–1425.

Knudsen EI, Konishi M (1980) Monaural occlusion shifts receptive-field locations of auditory midbrain units in the owl. J Neurophysiol 44:687–695.

Knudsen EI, Esterly SD, Knudsen PF (1984b) Monaural occlusion alters sound localization during a sensitive period in the barn owl. J Neurosci 4:11.

Kopp-Scheinpflug C, Tozer AJB, Robinson SW, Tempel BL, Hennig MH, Forsythe ID (2011) The Sound of Silence: Ionic Mechanisms Encoding Sound Termination. Neuron 71:911–925.

Kumpik DP, Campbell C, Schnupp JWH, King AJ (2019) Re-weighting of Sound Localization Cues by Audiovisual Training. Front Neurosci 13:1164.

Kumpik DP, Kacelnik O, King AJ (2010) Adaptive Reweighting of Auditory Localization Cues in Response to Chronic Unilateral Earplugging in Humans. J Neurosci 30:4883–4894.

Kuwada S, Batra R, Yin TCT, Oliver DL, Haberly LB, Stanford TR (1997) Intracellular Recordings in Response to Monaural and Binaural Stimulation of Neurons in the Inferior Colliculus of the Cat. J Neurosci 17:7565–7581.

Kwee IL, Matsuzawa H, Nakada K, Fujii Y, Nakada T (2017) Inferior colliculus syndrome: Clinical magnetic resonance microscopy anatomic analysis on a 7 T system. SAGE Open Med Case Rep 5:2050313X1774520.

Ledoux JE, Ruggiero DA, Forest R, Stornetta R, Reis DJ (1987) Topographic organization of convergent projections to the thalamus from the inferior colliculus and spinal cord in the rat. J Comp Neurol 264:123–146.

Li N, Gittelman JX, Pollak GD (2010) Intracellular Recordings Reveal Novel Features of Neurons That Code Interaural Intensity Disparities in the Inferior Colliculus. J Neurosci 30:14573–14584.

Li N, Pollak GD (2013) Circuits That Innervate Excitatory-Inhibitory Cells in the Inferior Colliculus Obtained with In Vivo Whole Cell Recordings. J Neurosci 33:6367–6379.

Litovsky RY, Fligor BJ, Tramo MJ (2002) Functional role of the human inferior colliculus in binaural hearing. Hear Res 165:177–188.

Liu Y, Li Y, Peng Y, Yu H, Xiao Z (2022) Bilateral Interactions in the Mouse Dorsal Inferior Colliculus Enhance the Ipsilateral Neuronal Responses and Binaural Hearing. Front Physiol 13:854077.

Lu Y, Jen PH-S (2003) Binaural interaction in the inferior colliculus of the big brown bat, Eptesicus fuscus. Hear Res 177:100–110.

Maaten L van der, Hinton G (2008) Visualizing Data using t-SNE. J Mach Learn Res 9:2579–2605.

Masterton RB, Jane JA, Diamond IT (1968) Role of brain-stem auditory structures in sound localization. II. Inferior colliculus and its brachium. J Neurophysiol 31:96–108.

Middlebrooks J, Pettigrew D (1981) Functional classes of neurons in primary auditory cortex of the cat distinguished by sensitivity to sound location. J Neurosci 1.

Middlebrooks JC (1987) Binaural mechanisms of spatial tuning in the cat's superior colliculus distinguished using monaural occlusion. J Neurophysiol 57:688–701.

Mogdans J, Knudsen EI (1993) Early monaural occlusion alters the neural map of interaural level differences in the inferior colliculus of the barn owl. Brain Res 619:29–38.

Moore DR, Hine JE, Jiang ZD, Matsuda H, Parsons CH, King AJ (1999) Conductive Hearing Loss Produces a Reversible Binaural Hearing Impairment. J Neurosci 19:8704–8711.

Moore DR, Irvine DRF (1981) Plasticity of binaural interaction in the cat inferior colliculus. Brain Res 208:198–202.

Moore M, Caspary D (1983) Strychnine blocks binaural inhibition in lateral superior olivary neurons. J Neurosci 3:237–242.

Musicant AD, Butler RA (1980) Monaural localization: An analysis of practice effects. Percept Psychophys 28:236–240.

Nakamoto KT, Jones SJ, Palmer AR (2008) Descending Projections From Auditory Cortex Modulate Sensitivity in the Midbrain to Cues for Spatial Position. J Neurophysiol 99:2347–2356.

Oberle HM, Ford AN, Czarny JE, Rogalla MM, Apostolides PF (2023) Recurrent circuits amplify corticofugal signals and drive feedforward inhibition in the inferior colliculus. J Neurosci:JN-RM-0626-23.

Oberle HM, Ford AN, Dileepkumar D, Czarny JE, Apostolides PF (2022) Synaptic mechanisms of top-down control in the non-lemniscal inferior colliculus. eLife 10:e72730.

Ono M, Oliver DL (2014) The Balance of Excitatory and Inhibitory Synaptic Inputs for Coding Sound Location. J Neurosci 34:3779–3792.

Orton LD, Papasavvas CA, Rees A (2016) Commissural Gain Control Enhances the Midbrain Representation of Sound Location. J Neurosci 36:4470–4481.

Pachitariu M, Stringer C, Dipoppa M, Schröder S, Rossi LF, Dalgleish H, Carandini M, Harris KD (2017) Suite2p: beyond 10,000 neurons with standard two-photon microscopy. bioRxiv 061507.

Palmer AR, King AJ (1985) A monaural space map in the guinea-pig superior colliculus. Hear Res 17:267–280.

Panniello M, King AJ, Dahmen JC, Walker KMM (2018) Local and Global Spatial Organization of Interaural Level Difference and Frequency Preferences in Auditory Cortex. Cereb Cortex 28:350–369.

Park TJ, Pollak GD (1993) GABA shapes sensitivity to interaural intensity disparities in the mustache bat's inferior colliculus: implications for encoding sound location. J Neurosci 13:2050–2067.

Park TJ, Pollak GD (1994) Azimuthal receptive fields are shaped by GABAergic inhibition in the inferior colliculus of the mustache bat. J Neurophysiol 72:1080–1102.

Poirier P, Samson FK, Imig TJ (2003) Spectral Shape Sensitivity Contributes to the Azimuth Tuning of Neurons in the Cat's Inferior Colliculus. J Neurophysiol 89:2760–2777.

Quass GL, Rogalla MM, Ford AN, Apostolides PF (2024) Mixed representations of sound and action in the auditory midbrain. J Neurosci:e1831232024.

Rajan R, Aitkin LM, Irvine DR (1990) Azimuthal sensitivity of neurons in primary auditory cortex of cats. II. Organization along frequency-band strips. J Neurophysiol 64:888–902.

Ramamurthy DL, Recanzone GH (2017) Spectral and spatial tuning of onset and offset response functions in auditory cortical fields A1 and CL of rhesus macaques. J Neurophysiol 117:966–986.

Remington ED, Wang X (2019) Neural Representations of the Full Spatial Field in Auditory Cortex of Awake Marmoset (*Callithrix jacchus*). Cereb Cortex 29:1199–1216.

Robinson NTM, Descamps LAL, Russell LE, Buchholz MO, Bicknell BA, Antonov GK, Lau JYN, Nutbrown R, Schmidt-Hieber C, Häusser M (2020) Targeted Activation of Hippocampal Place Cells Drives Memory-Guided Spatial Behavior. Cell 183:1586-1599.e10.

Rose JE, Gross NB, Geisler CD, Hind JE (1966) Some neural mechanisms in the inferior colliculus of the cat which may be relevant to localization of a sound source. J Neurophysiol 29:288–314.

Rule ME, O'Leary T, Harvey CD (2019) Causes and consequences of representational drift. Curr Opin Neurobiol 58:141–147.

Samson FK, Barone P, Clarey JC, Imig TJ (1994) Effects of ear plugging on single-unit azimuth sensitivity in cat primary auditory cortex. II. Azimuth tuning dependent upon binaural stimulation. J Neurophysiol 71:2194–2216.

Samson FK, Barone P, Irons WA, Clarey JC, Poirier P, Imig TJ (2000) Directionality derived from differential sensitivity to monaural and binaural cues in the cat's medial geniculate body. J Neurophysiol 84:1330–1345.

Sanchez Jimenez A, Willard KJ, Bajo VM, King AJ, Nodal FR (2023) Persistence and generalization of adaptive changes in auditory localization behavior following unilateral conductive hearing loss. Front Neurosci 17:1067937.

Sanes DH, Malone BJ, Semple MN (1998) Role of Synaptic Inhibition in Processing of Dynamic Binaural Level Stimuli. J Neurosci 18:794–803.

Schnupp JWH, King AJ (1997) Coding for Auditory Space in the Nucleus of the Brachium of the Inferior Colliculus in the Ferret. J Neurophysiol 78:2717–2731.

Scholl B, Gao X, Wehr M (2010) Nonoverlapping Sets of Synapses Drive On Responses and Off Responses in Auditory Cortex. Neuron 65:412–421.

Sheintuch L, Rubin A, Brande-Eilat N, Geva N, Sadeh N, Pinchasof O, Ziv Y (2017) Tracking the Same Neurons across Multiple Days in Ca2+ Imaging Data. Cell Rep 21:1102–1115.

Shi K, Quass GL, Rogalla MM, Ford AN, Czarny JE, Apostolides PF (2024) Population coding of time-varying sounds in the nonlemniscal inferior colliculus. J Neurophysiol 131:842–864.

Shinn-Cunningham B (2001) Models of Plasticity in Spatial Auditory Processing. Audiol Neurootol:5.

Slattery WH III, Middlebrooks JC (1994) Monaural sound localization: acute versus chronic unilateral impairment. Hear Res. 75(1-2):38-46.

Slee SJ, Young ED (2013) Linear Processing of Interaural Level Difference Underlies Spatial Tuning in the Nucleus of the Brachium of the Inferior Colliculus. J Neurosci 33:3891–3904.

Slee SJ, Young ED (2014) Alignment of sound localization cues in the nucleus of the brachium of the inferior colliculus. J Neurophysiol 111:2624–2633.

Snapp HA, Ausili SA (2020) Hearing with One Ear: Consequences and Treatments for Profound Unilateral Hearing Loss. J Clin Med 9:1010.

Thornton JL, Anbuhl KL and Tollin DJ (2021) Temporary Unilateral Hearing Loss Impairs Spatial Auditory Information Processing in Neurons in the Central Auditory System. *Front. Neurosci.* 15:721922.

Town SM, Brimijoin WO, Bizley JK (2017) Egocentric and allocentric representations in auditory cortex Ungerleider L, ed. PLOS Biol 15:e2001878.

Valtcheva S, Issa HA, Bair-Marshall CJ, Martin KA, Jung K, Zhang Y, Kwon H-B, Froemke RC (2023) Neural circuitry for maternal oxytocin release induced by infant cries. Nature 621:788–795.

van den Wildenberg MF, Bremen P (2024) Heterogeneous spatial tuning in the auditory pathway of the Mongolian Gerbil (Meriones unguiculatus). Eur J Neurosci. 60(5):4954-4981.

Wenstrup JJ, Fuzessery ZM, Pollak GD (1988) Binaural neurons in the mustache bat's inferior colliculus. II. Determinants of spatial responses among 60-kHz EI units. J Neurophysiol 60:1384–1404.

Wilmington D, Gray L, Jahrsdoerfer R (1994) Binaural processing after corrected congenital unilateral conductive hearing loss. Hear Res 74:99–114.

Winer JA, Larue DT, Diehl james J, Hefti BJ (1998) Auditory cortical projections to the cat inferior colliculus. J Comp Neurol 400:28.

Wong AB, Borst JGG (2019) Tonotopic and non-auditory organization of the mouse dorsal inferior colliculus revealed by two-photon imaging. eLife 8:e49091.

Wong K, Kozin ED, Kanumuri VV, Vachicouras N, Miller J, Lacour S, Brown MC, Lee DJ (2019) Auditory Brainstem Implants: Recent Progress and Future Perspectives. Front Neurosci 13:10.

943 Wood KC, Town SM, Bizley JK (2019) Neurons in primary auditory cortex represent sound source
944 location in a cue-invariant manner. Nat Commun 10:3019.

945 Wright BA, Fitzgerald MB (2001) Different patterns of human discrimination learning for two interaural
946 cues to sound-source location. Proc Natl Acad Sci 98:12307–12312.

947 Xiong XR, Liang F, Li H, Mesik L, Zhang KK, Polley DB, Tao HW, Xiao Z, Zhang LI (2013) Interaural
948 Level Difference-Dependent Gain Control and Synaptic Scaling Underlying Binaural
949 Computation. Neuron 79:738–753.

950 Xiong XR, Liang F, Zingg B, Ji X, Ibrahim LA, Tao HW, Zhang LI (2015) Auditory cortex controls sound-
951 driven innate defense behaviour through corticofugal projections to inferior colliculus. Nat
952 Commun 6:7224.

953 Yao JD, Bremen P, Middlebrooks JC (2013) Rat primary auditory cortex is tuned exclusively to the
954 contralateral hemifield. J Neurophysiol 110:2140–2151.

955 Yin TCT, Smith PH, Joris PX. (2019) Neural Mechanisms of Binaural Processing in the Auditory
956 Brainstem. Compr Physiol. 9(4):1503-1575.

957 Zhao X, Chen H, Liu X, Cang J (2013) Orientation-selective Responses in the Mouse Lateral
958 Geniculate Nucleus. J Neurosci 33:12751–12763.

959 Zheng W, Knudsen EI (1999) Functional Selection of Adaptive Auditory Space Map by GABA $_A$ -
960 Mediated Inhibition. Science 284:962–965.

961 Zonooz B, Van Opstal AJ (2019) Differential Adaptation in Azimuth and Elevation to Acute Monaural
962 Spatial Hearing after Training with Visual Feedback. eNeuro 6:ENEURO.0219-19.2019.

963 Zrull MC, Coleman JR (1997) Effects of Tectal Grafts on Sound Localization Deficits Induced by Inferior
964 Colliculus Lesions in Hooded Rats. Exp Neurol 145:16–23.

965

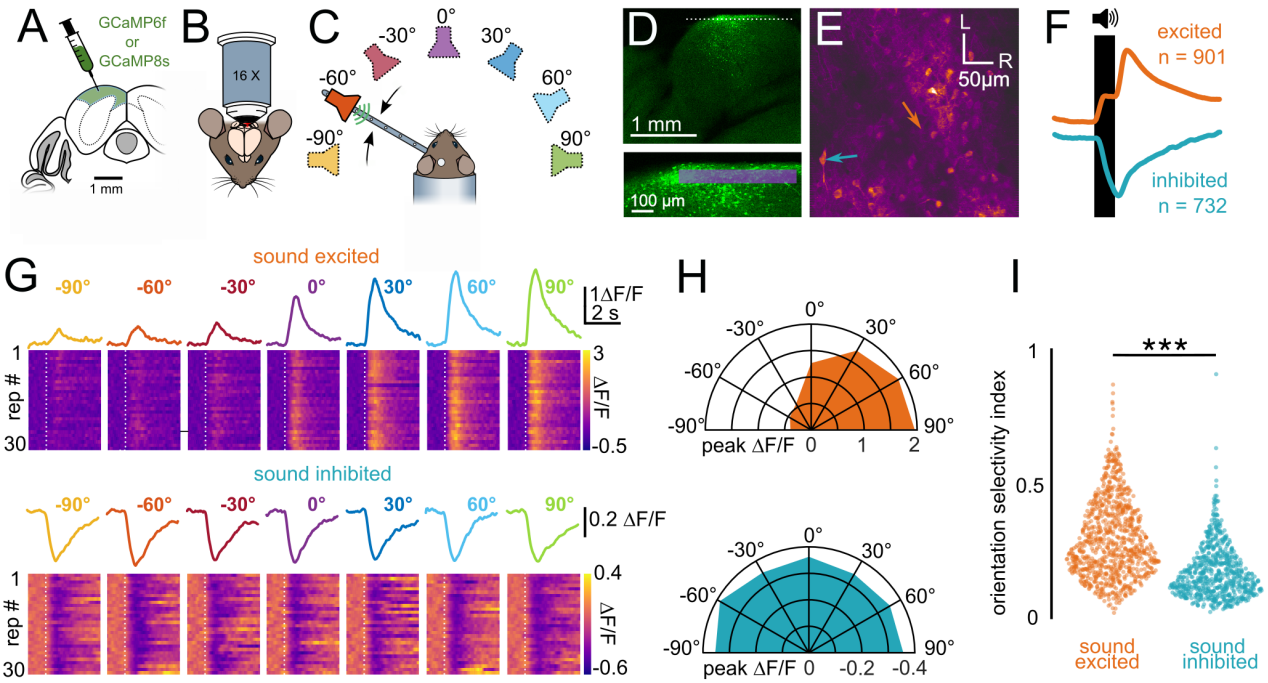

Figure 1: *2-photon Ca^{2+} imaging of spatial sound responses in dorsal shell IC neurons of awake mice*
A) Schematic of experiment. We injected an adeno-associated virus to express genetically encoded Ca^{2+} indicators (GCaMP6f or GCaMP8s) in the left IC of mice. **B)** Following recovery from surgery, 2-photon Ca^{2+} imaging was conducted in the superficial layers of the left IC in awake, head-fixed mice. **C)** During imaging sessions, sounds were presented at specific angles across the frontal azimuth via a servo-motor based movable speaker system. **D)** Example confocal microscopy section showing GCaMP8s expression in the left shell IC. L = Lateral; R = Rostral. Lower panel: The area denoted by the dotted line is shown at higher magnification. Rectangle denotes range of depths for the imaged FOVs across all mice. **E)** Example FOV: Orange and blue arrows respectively denote example sound excited and sound inhibited neurons shown in more detail in panel G. **F)** Mean fluorescence waveform across all trials and all neurons, for sound excited and sound inhibited populations identified via t-SNE clustering (orange and blue, respectively). Black bar denotes sound presentation time of 0.5 s broadband noise burtsts **G)** Example data from single sound excited (top) and sound inhibited (bottom) neurons from panel E. Fluorescence traces are averages of 30 repetitions at each presentation angle, whereas the heatmaps show single trial responses. **H)** Polar plots of fluorescence amplitudes for the example neurons in panel G. **I)** Summary of OSI values for sound excited and sound inhibited neurons (orange and blue, respectively).

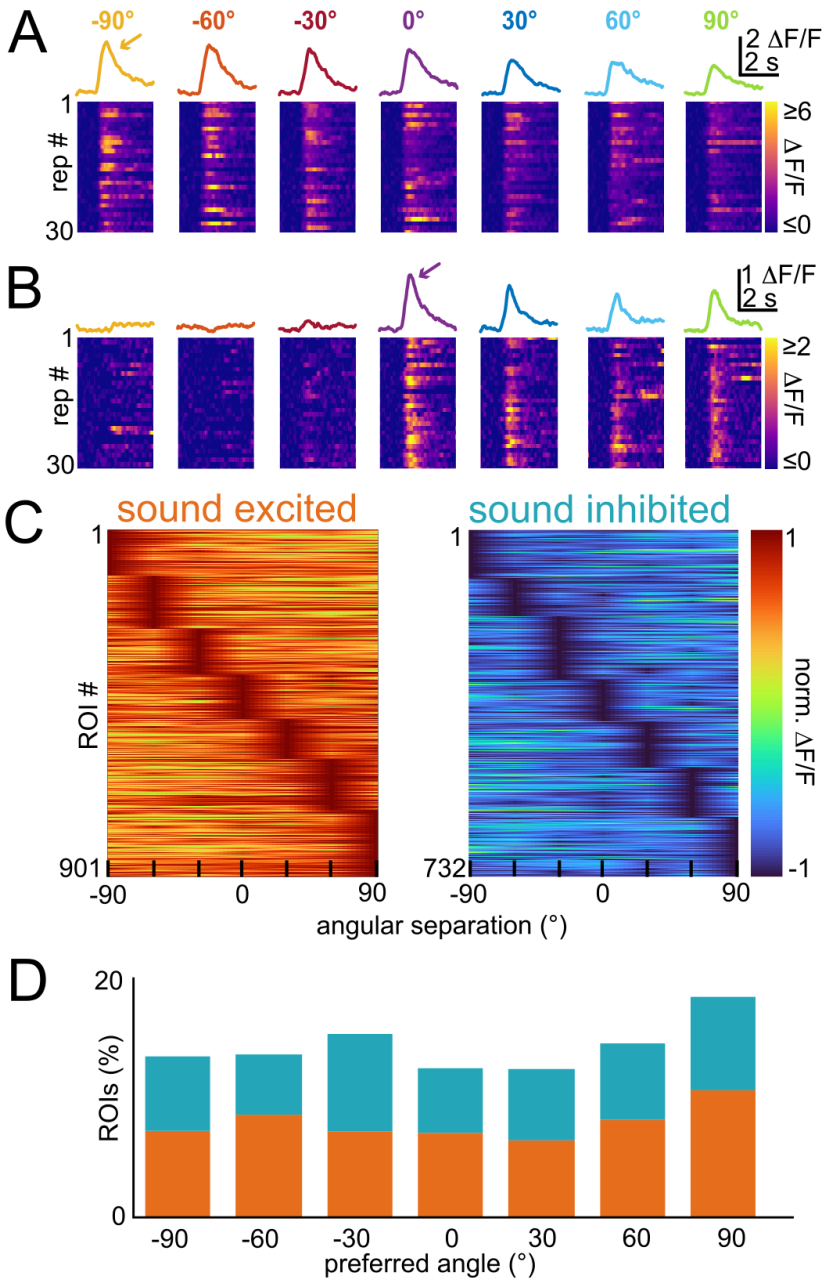

Figure 2: *Rich and diverse spatial tuning profiles of dorsal shell IC neurons*
A) Example sound excited neuron with preferred responses in the ipsilateral hemifield. Fluorescence traces are averages across all presentations at a particular angle. Heatmaps show individual trials. Arrow denotes preferred position defined as the highest average peak response at -90°. **B)** Same as A, but for a neuron with a preferred position at the midline. **C)** Population distribution of preferred angles for sound excited (left, orange) and sound inhibited neurons (right, blue). **D)** Summary histogram of preferred angles for sound excited and sound inhibited neurons (orange and blue, respectively).

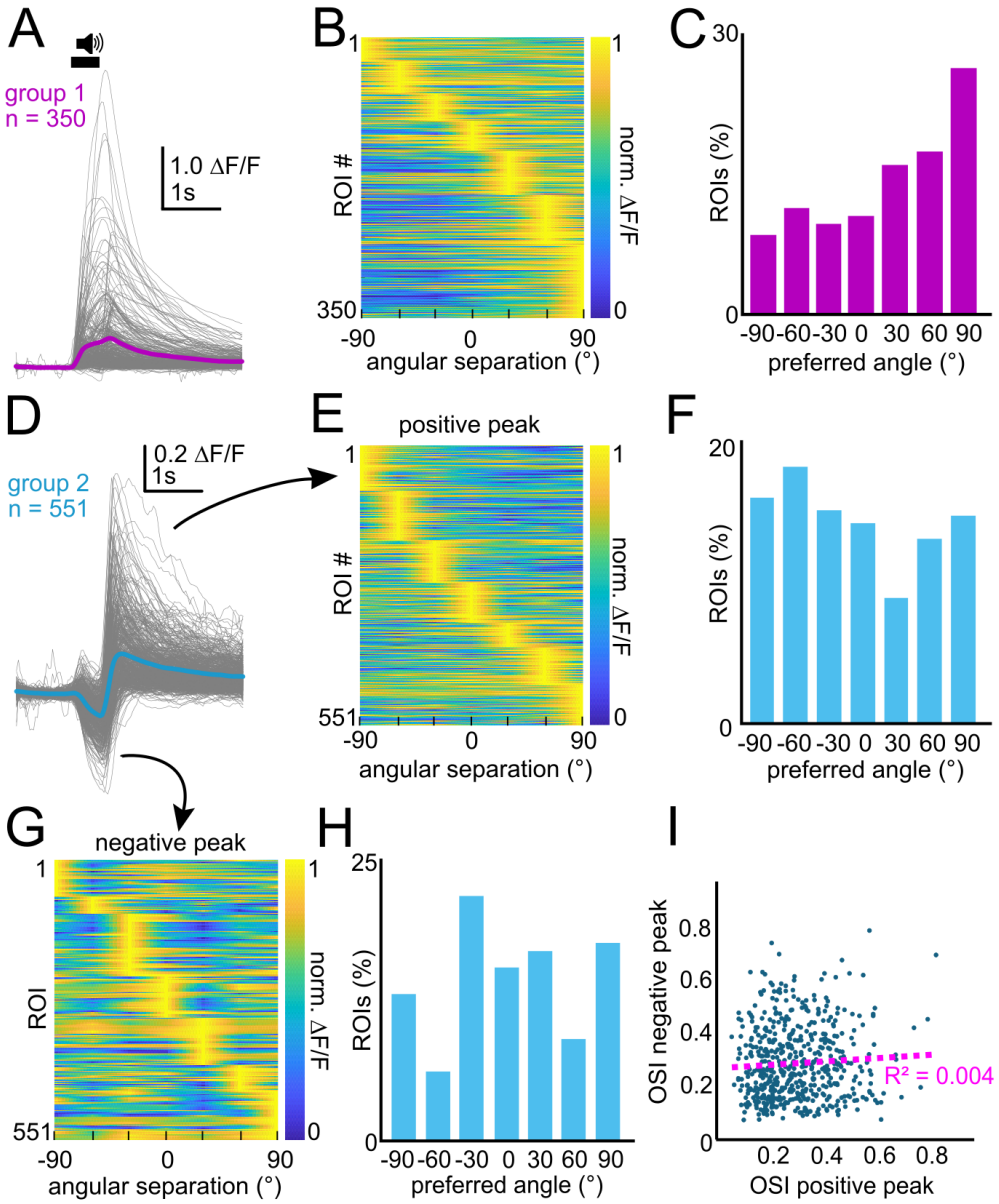

Figure 3: *Waveform characteristics and spatial selectivity of sound excited neurons*
A) Average waveforms of neurons clustered into group 1 with one positive peak following sound presentation (n =350), purple line denotes the average waveform over all neurons within this cluster. **B)** Population distribution of preferred angles for neurons in A. **C)** Summary histogram of preferred angles for neurons given in A. **D)** Average waveforms of neurons clustered into group 2 with one negative and positive peak following sound presentation (n =551), blue line denotes the average waveform over all neurons within this cluster. **E)** Population distribution of preferred angles for the positive peak of neurons in D. **F)** Summary histogram of preferred angles for the positive peak of neurons given in D. **G)** Population distribution of preferred angles for the negative peak of neurons in D. **H)** Summary histogram of preferred angles for the negative peak of neurons given in D. **I)** correlation of OSI values for positive and negative peaks of group 2 neurons.

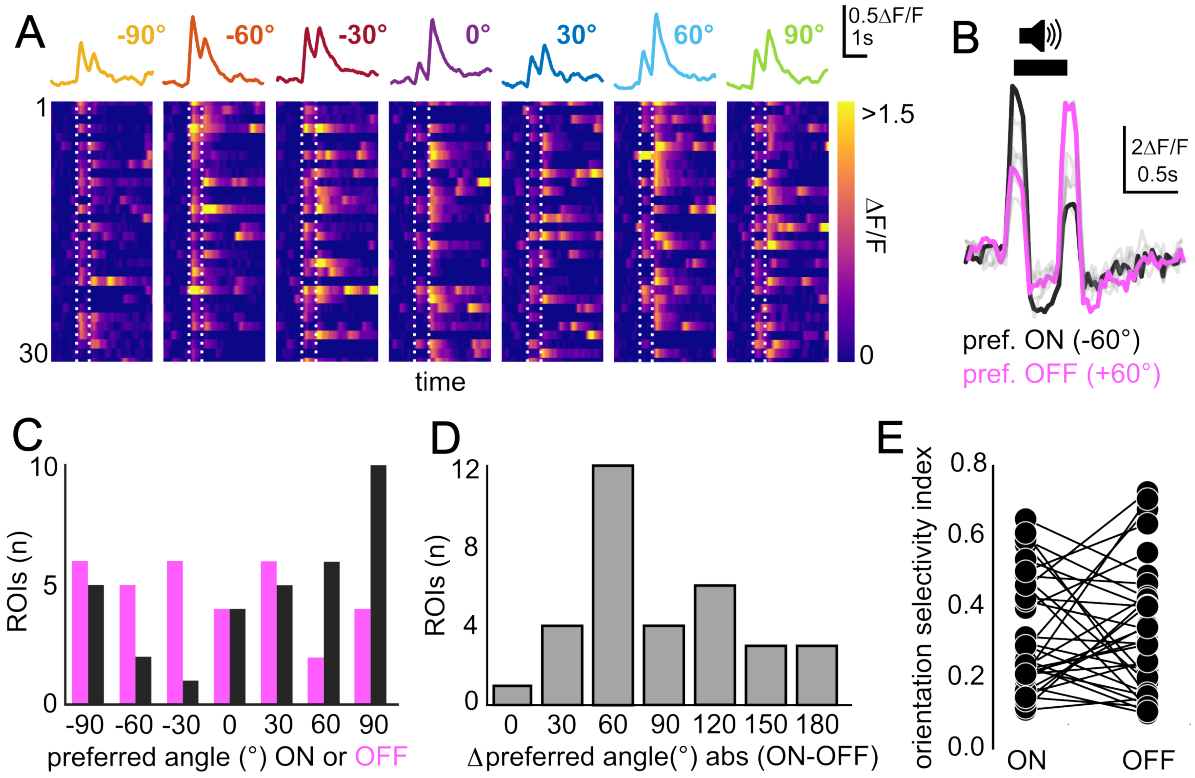

Figure 4: *ON and OFF excitation can exhibit distinct spatial tuning in single neurons.* **A)** Average fluorescence traces (top) and single trials (lower panel, heatmaps) for an example neuron showing ON and OFF excitatory responses. **B)** the first derivative of the fluorescence traces from panel A are overlaid. Black bar is sound presentation. Preferred ON and OFF responses are highlighted in black and magenta, respectively. **C)** Population distribution of preferred ON and OFF responses (black and magenta, respectively) for n = 33 neurons as in panel A. **D)** Absolute difference in preferred angles for ON and OFF responses in the same neurons. **E)** OSI values for ON and OFF excitation in the same neurons.

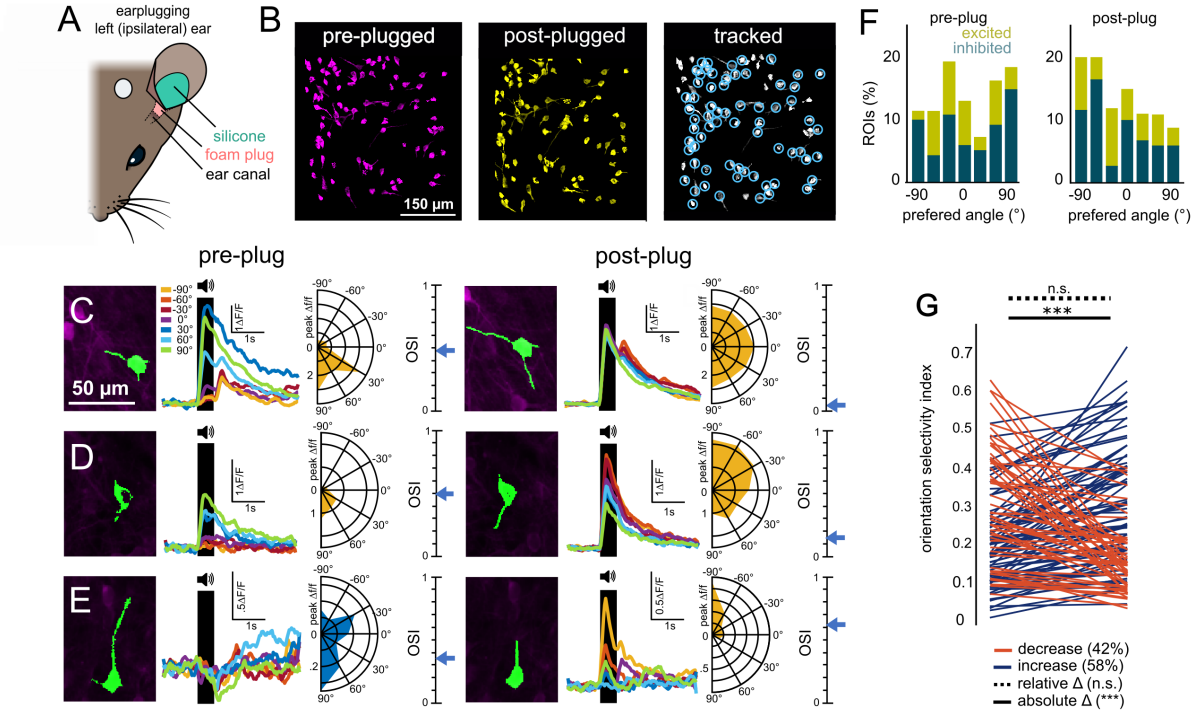

Figure 5: *Ipsilateral ear plugging alters spatial receptive fields in dorsal shell IC neurons*
A) Mice were fit with a monaural foam plug into the left ear, subsequently sealed with silicone. **B)** The same FOV was imaged pre (left, magenta) and post (middle, yellow) monaural conductive hearing loss. ROIs of both FOVs (pre and post condition) were tracked across sessions. **C)** Example neuron which broadened its receptive field following ipsilateral ear plugging: Panels 1-4 show the pre plugged condition, panels 5-8 give the post-plugged condition for the same neuron. **D)** Example neuron showing broadened selectivity and switching of preferred azimuthal hemifield following monaural ear plugging. **E)** Example neuron which changes from sound inhibited to sound excited following ear plugging. **F)** Summary histograms of preferred angles for sound-excited (green) and sound-inhibited (teal) neurons, pre- and post-plugging (upper and lower panels, respectively). **G)** Change in orientation selectivity following monaural ear plugging. Neurons either increase (blue lines, (58%) or decrease (orange lines, 42 %) orientation selectivity following monaural ear plugging.

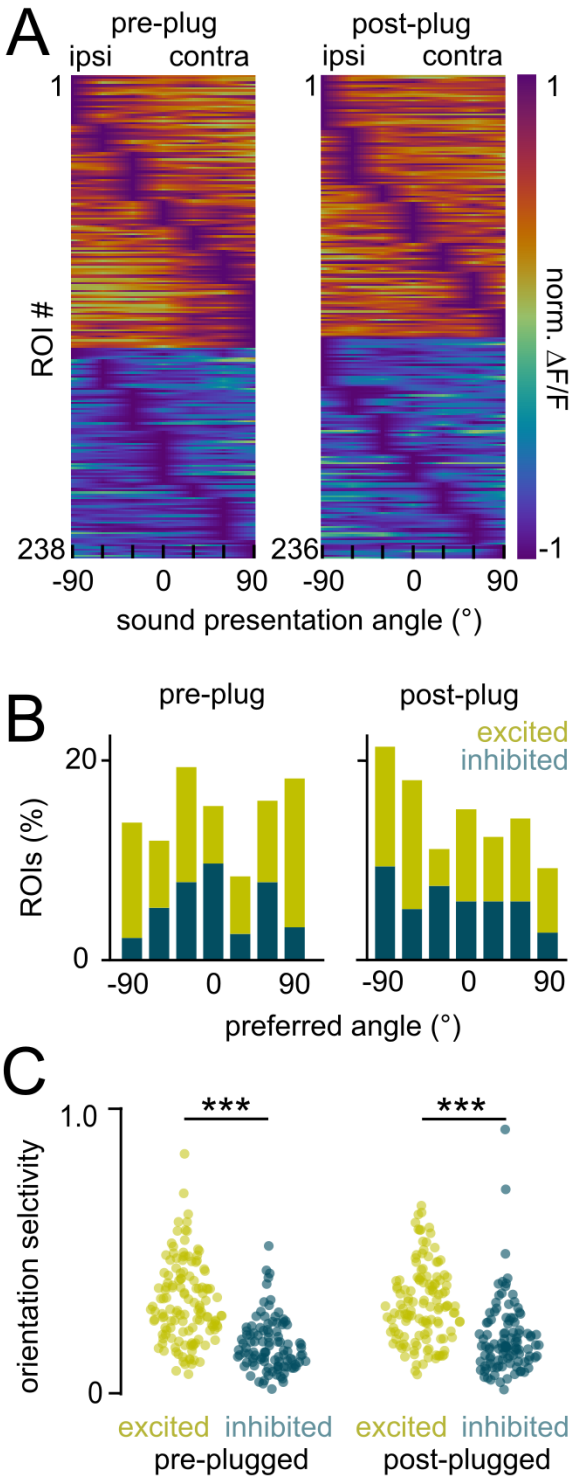

Figure 6: *Population code of auditory space in the dorsal shell IC is maintained across conditions of typical and altered binaural hearing*

A) Population distribution of preferred angles for neurons in pre- (left) and post-plugged (right) conditions **B)** Summary histogram of preferred angles for neurons given in A, divided into sound excited (green) and inhibited neurons (teal) **C)** Summary of OSI values for sound excited and sound inhibited neurons (green and blue, respectively) for neurons given in A.

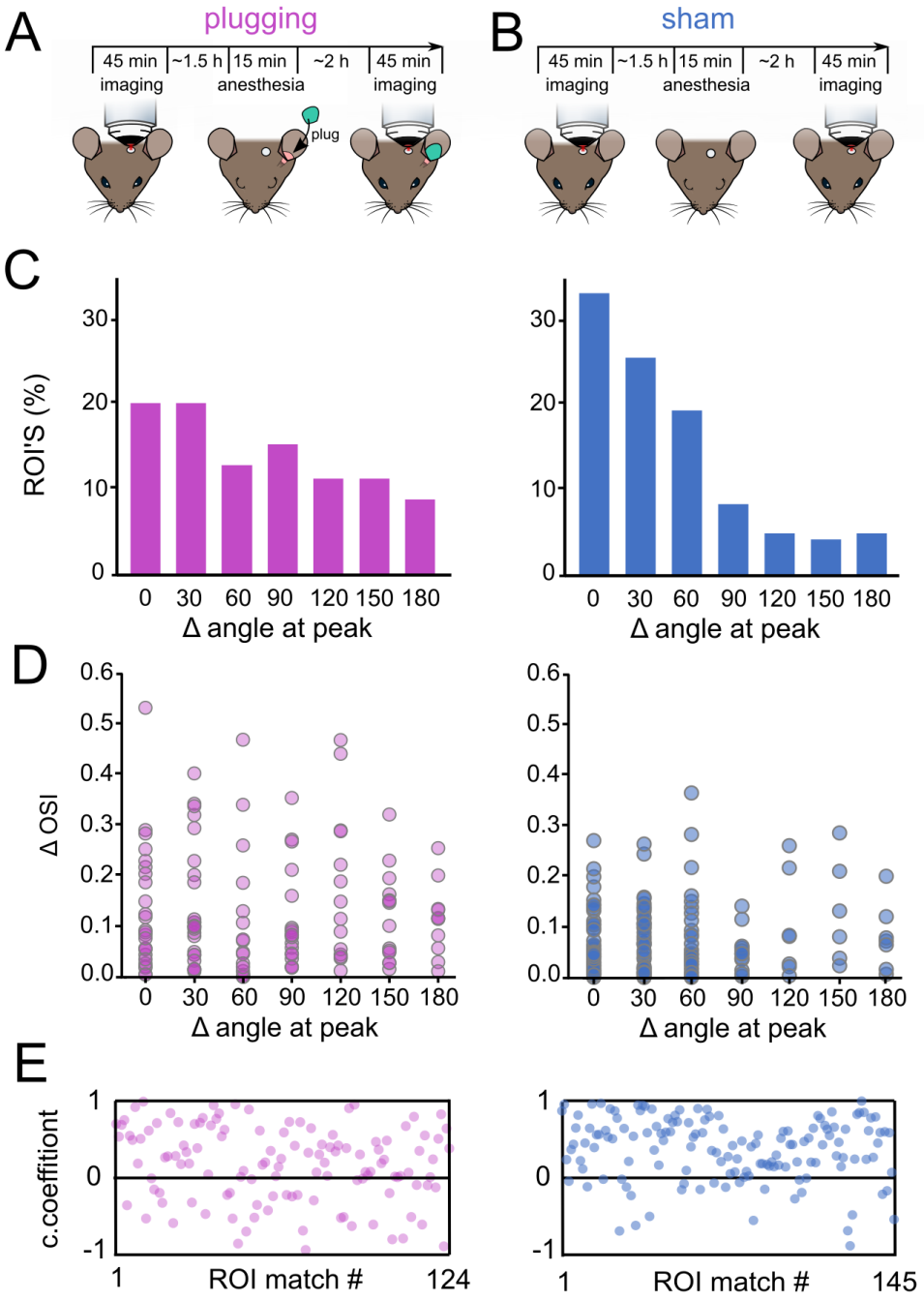

Figure 7: *Comparison of spatial tuning changes in ear plugged and sham operated mice.*
A,B) Timelines for experimental (A) and sham mice (B). **C)** Distribution of sound presentation angles pre- and post-plugging (left matched heatmaps) and for pre- and post-sham conditions (right matched heatmaps). **D)** Quantitative analysis of the change in orientation selectivity index (Δ OSI), plotted over the change in change in preferred peak given in degree (Δ angle at peak) for experiment (left, magenta) and sham (right, blue). **E)** Summary histograms of changes in preferred peak given in degree (Δ angle at peak) for experiment (left, magenta) and sham (right, blue). **F)** Correlation of single cell tuning curves across pre and post conditions for experiment (left, magenta) and sham (right, blue).

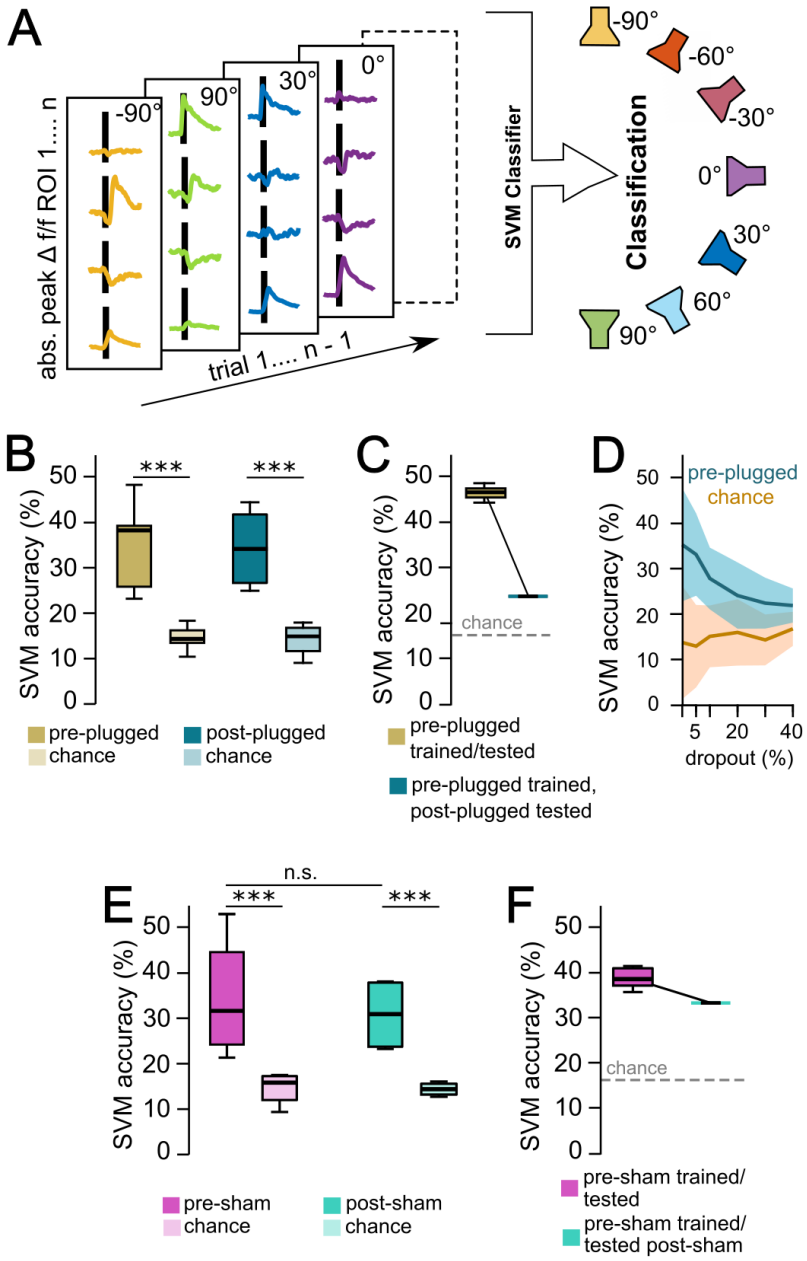

Figure 8: *Population decoding of sound presentation angle from pre and post plugged data using support vector machine analysis*
A) SVM classifiers were trained to predict sound angle on a trial-by-trial basis using the absolute fluorescence peak in each neuron (leave-one-out method). A linear kernel and the sequential minimal optimization were used as SVM parameters. **B)** Sound angle decoding accuracy for SVM classifiers trained and tested on data obtained from either pre-plugged (golden boxes) or post-plugged (teal boxes) mice. Chance levels were obtained from shuffling the trial fluorescence data and trial sound angles before training. **C)** Same as B, but for trackable neurons pooled across all animals, comparing accuracy from classifiers trained and tested on data from pre plugged mice with those trained on data from pre plugged mice and tested on data from post plugged mice. Chance level is theoretical for uniform classification. **D)** Decoding accuracy plotted over size of dropout layer (proportion of random neurons per trial not used for classification) as mean and standard deviation for pre-plugged (teal) data and shuffled data (orange, chance level). **E)** Same as B, but for sham-treated control mice. **F)** Same as C, but for sham-treated control mice. *** indicates $p < 0.001$.

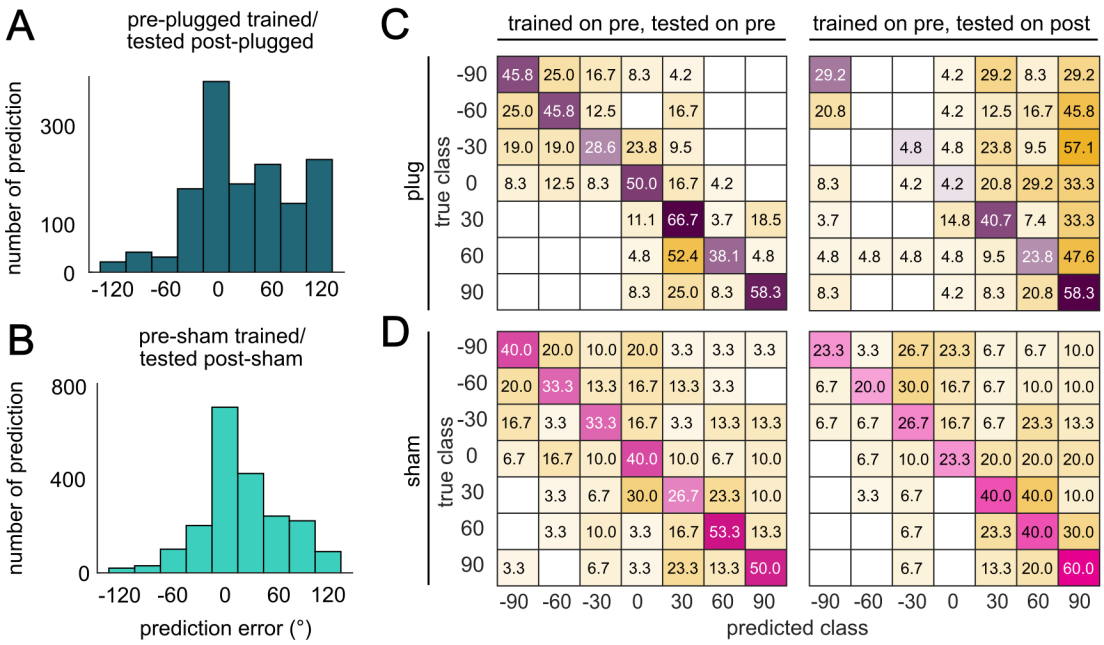

Figure 9: *SVM classifier decoding errors are biased towards the contralateral side*
A) Prediction error histogram for an SVM classifier trained on data from trackable neurons pre-plugged, pooled across all mice, and tested on data from the same neurons post-plugged. **B)** The same as A, but for sham-treated control mice. **C)** Confusion matrices for experimental mice for the classifier trained and tested on pre-plugged data (left), or trained on pre-plugged and tested on post-plugged data (right). Purple and orange entries are correct and incorrect predictions, respectively. Numbers indicate the proportion of predicted angles per true sound presentation angle in % (Rows add up to 100%). **D)** The same as C, but for sham-treated control mice.